Nano Research
2022, 15(12): 9985–10005

ISSN 1998-0124 CN 11-5974/O4
https://doi.org/10.1007/s12274-022-4795-3

Review Article

Advances of photothermal chemistry in photocatalysis, thermocatalysis, and synergetic photothermocatalysis for solar-to-fuel generation

Minmin Gao[1], Tianxi Zhang[2], and Ghim Wei Ho[1,3] (✉)

[1] *Department of Electrical and Computer Engineering, National University of Singapore, 4 Engineering Drive 3, Singapore 117583, Singapore*
[2] *Department of Chemical and Biomolecular Engineering, National University of Singapore, 4 Engineering Drive 4, Singapore 117585, Singapore*
[3] *Institute of Materials Research and Engineering, Agency for Science, Technology and Research (A*STAR), 3 Research Link, Singapore 117602, Singapore*

Received: 10 May 2022 / **Revised:** 18 July 2022 / **Accepted:** 20 July 2022

ABSTRACT

The urgency of reducing pollutants and greenhouse gas emissions while maintaining fuel supply for the development of society remains one of the greatest challenges. Solar energy, a clean and sustainable energy resource, can be converted into fuels through solar-driven catalysis, and this provides an attractive solution for future energy demand. The current development of photothermal catalysis (PTC) based on the integration of solar thermal and photochemical contributions is becoming increasingly popular for full spectrum utilization. The combination of the thermochemical and photochemical processes synergistically drives the catalytic reactions efficiently under relatively mild conditions. In this review, the mechanisms of PTC are classified based on driving forces and the benefits of photothermal effects in different PTC reactions are discussed. Subsequently, the techniques for differentiating and quantifying the various effects of PTC, including experimental designs, thermometry characterization techniques, and computational studies, are summarized. Then, the major determinant properties and architectural designs for efficient photothermal catalysts are offered. Moreover, applications for fuel generation through water splitting and carbon dioxide reduction are reviewed. Finally, the current challenges and future directions of PTC are presented. This article aims to provide a comprehensive review of the current advances in PTC along with a guide for understanding the mechanisms and rational material designs to pursue solar fuel that would diversify and increase the sustainability of our energy supply.

KEYWORDS

photothermal chemistry, photocatalysis, thermocatalysis, water splitting, CO_2 conversion, solar fuel

1 Introduction

Fossil fuels have been the primary energy that drives modern civilization for over 150 years. As the energy demand continues to increase for human activities, limited fossil fuels cannot provide a long-term solution for the energy crisis. Besides, the damaging effects of fossil fuels on the environment and the global climate due to the release of pollutants and greenhouse gasses are alarming to humanity. Accordingly, solar energy as the most abundant renewable resource appears to be a favourable option for the energy needs and the transition to a sustainable future. Solar energy manifests in the form of both light and heat, which can be converted through photoelectric and/or photothermal processes to generate power (electricity) and chemical energy (fuels) [1–3]. Although electricity generated from the photovoltaic process has been successfully commercialized, it faces the challenge in energy storage due to the dispersed and intermittent nature of sunlight. In contrast, solar fuels produced through catalytic pathways store solar energy in the form of chemical bonds, which makes them available on demand. These fuels including hydrogen fuel from water splitting and carbon-based fuels from carbon dioxidereduction can be generated via both photochemical and thermochemical processes. Recently, photothermal catalysis (PTC), which utilizes both light and heat contributions of the sun, has been developed to synergistically enhance photocatalysis and/or thermocatalysis for fuel production [4–6]. Compared to the pure photocatalytic system which suffers from low spectral efficiency limited by the bandgap of photocatalyst, PTC extends the absorption range to fully utilize the solar spectrum and promotes the reaction rate [7–9]. On the other hand, introducing PTC in a conventional thermocatalytic system provides an alternative heating means to reduce the high energy input, and drive catalytic reactions more efficiently under relatively mild conditions [10–12]. The synergetic effect of PTC by coupling both photochemistry and thermochemistry not only reveals a non-linear combined activity, but also demonstrates improved product selectivity and catalyst stability [13–16].

This synergistic effect of PTC has attracted significant attention in the field of catalysis and proliferated into diverse applications. However, most reviews that have been published focused mainly on PTC in either photocatalytic- or thermocatalytic-driven catalysis [17] with specific reactions [18–20] or materials [21, 22]. The rapid development in this emerging area, especially the

Address correspondence to elehgw@nus.edu.sg

integration of photochemistry and thermochemistry, requires comprehensive and in-depth review. Photothermal catalysis is a general term that has been used to refer to catalytic reactions involving the combination of light and heat. Currently, there is a lack of a comprehensive classification of the different mechanisms involved in these reactions, which brings confusion and ambiguity. In this review (Fig. 1), the classification of various mechanisms of PTC is first introduced and defined. Then various photothermal enhancement effects of PTC including efficient light and energy utilization, boosted catalytic activity through localized heating, promoted reaction kinetics, increased mass transfer, enhanced selectivity of products, and improved stability of the catalyst are discussed. Furthermore, methodologies to study the reaction mechanisms of photothermal processes are identified concerning experimental design, thermometry measurement, and theoretical simulation. Also, requirements for photothermal catalyst design including enhancing light absorption, optimizing photothermal conversion efficiency, confining heat at the reaction sites, increasing the number of active sites, and constructing preferable photoinduced carrier generation and transfer path are emphasized. In addition, applications for fuel generation, both hydrogen fuel from water splitting and carbon-based fuels from carbon dioxide reduction, are summarized. Lastly, conclusion and perspective of PTC are presented. This review aims to highlight the recent advancements of PTC for fuel generation via both photochemical and/or thermochemical processes. It offers a better understanding of the fundamental mechanisms and insights into various photothermal enhancement effects in catalysis. Moreover, it provides a guide for photothermal catalyst design, methodologies, and future development in the area of catalytic fuel generation.

2 Fundamentals of photothermal catalysis

Photothermal effect has been primarily used for medical applications and recently widely applied to water evaporation, while adopting photothermal effect in catalysis is relatively a new field. The photothermal effect in medical applications and water evaporation is referred to as the conversion of incident light through photoexcitation resulting in partial or complete thermal energy production [23]. However, photothermal chemistry in catalysis cannot be merely understood as a thermal effect, as light has also been utilized as electromagnetic energy for photochemical processes in various catalysis reactions. In this section (Fig. 2), the classification of PTC for fuel generation is based on the driving force of the reaction, namely photochemistry, thermochemistry, and a combination of photo and thermo-chemistry. The mechanism and efficiency calculation of each type are evaluated to provide an overview of PTC in various reactions.

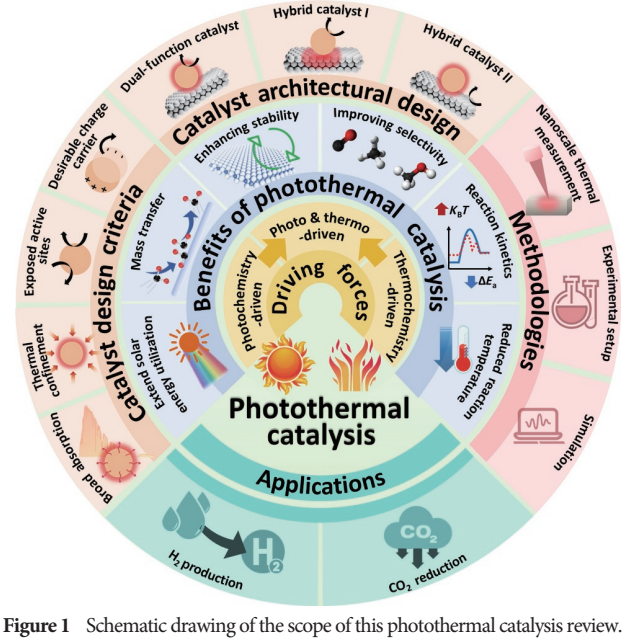

Figure 1 Schematic drawing of the scope of this photothermal catalysis review.

2.1 Classification

Photothermal catalysis often denotes the involvement of both light and heat in the catalytic process. However, the fundamental mechanisms can be based on photocatalytic, thermocatalytic, or a combination for fuel generation, which makes the PTC effect in each type of reaction to be distinct. Here, each type of reaction is clearly defined to facilitate the understanding of the photothermal effects in various reactions.

- **Photochemistry-driven photothermal catalysis (P-PTC)** supplies heat from light or external heating sources to the photocatalytic system. The thermal energy applied in this system enhances the photocatalytic activity but is incompetent to activate or drive the reaction. Thermocatalysis has an insignificant effect in this case [24].
- **Thermochemistry-driven photothermal catalysis (T-PTC)** introduces light as the heating source to the thermocatalytic system. Through the photothermal conversion process, heat generated from light is used to stimulate thermal reduction. It can either completely replace the conventional heating source or reduce the temperature required for the reaction. Photocatalysis plays an insubstantial role under such circumstances.
- **Synergetic photochemistry-thermochemistry-driven catalysis (S-PTC)** involves both photocatalytic and thermocatalytic reactions, achieving better performance than the arithmetic sum of individual photocatalytic and thermocatalytic activities with alleviating reaction condition demands. This synergetic effect also provides new pathways of catalysis which will be discussed in the following sections.

2.2 Mechanisms

It is noteworthy that photothermal chemistry brings different effects in various types of photothermal catalysis with distinct mechanisms. The reaction mechanisms of each type are summarized to provide a foundation for understanding the catalytic enhancements and designing efficient photothermal catalysts (Fig. 2).

2.2.1 Photothermal chemistry in P-PTC

Photocatalysis is the most direct route for solar-to-fuel conversion which requires a photoactive material to generate electrons at high-energy states upon photoexcitation, followed by charge separation and subsequent charge transfer to the active sites on the surface of the photocatalyst. In the conventional view, high temperature may adversely promote charge recombination, henceforth photocatalytic reactions are often carried out at room temperature or even lower temperature [5]. However, recently, the rising temperature at the active sites in photocatalysis with enhanced photoactivity has been demonstrated. Light used to activate the photocatalytic reaction normally requires higher energy photons in the ultraviolet (UV) or visible (vis) range of the spectrum. The lower energy photons in the near-infrared (NIR) region provide the thermal energy to enhance the photocatalytic activity through kinetic promotion, apparent activation energy reduction, adsorbed reactants in excited states augmentation, and/or diffusion of reactants and products improvement [25, 26]. These enhancements from the thermal effect may also be achieved by other external heating methods. The change of Gibbs free energy

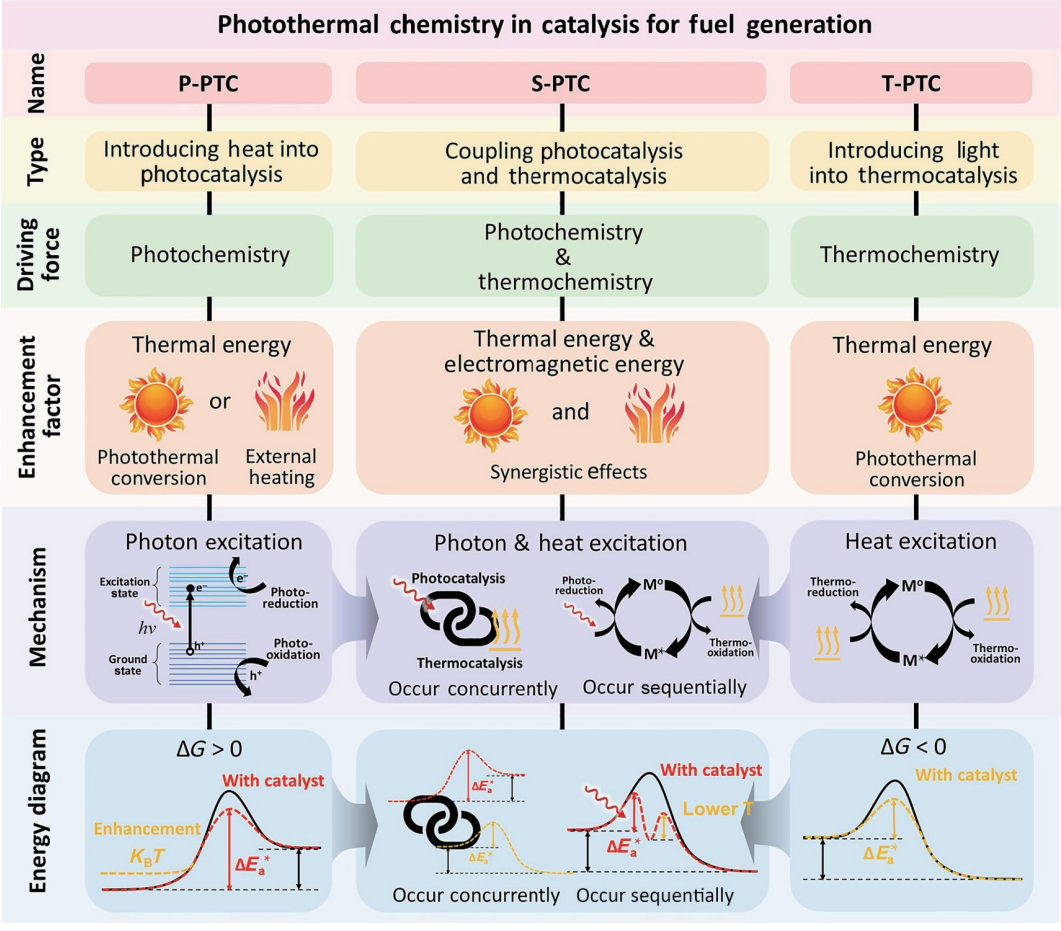

Figure 2 Classification of photothermal chemistry in catalysis for fuel generation.

(ΔG) for photochemical reaction can be positive ($\Delta G > 0$) or negative ($\Delta G < 0$). In this review, we only focus on catalysis for fuel generation, namely hydrogen generation from water and carbon dioxide reduction, and these reactions are thermodynamic uphill reactions, thus the change of Gibbs free energy is positive ($\Delta G > 0$) [27].

2.2.2 *Photothermal chemistry in T-PTC*

Another approach to solar fuel production is via thermochemistry. Unlike photocatalysis which can be operated under mild conditions, thermocatalysis is driven by high temperature and/or pressure with a redox material as the thermocatalyst. In thermocatalysis, the process involves the adsorption of reactant molecules, chemical bonds activation, intermediates formation, conversion of intermediates into products, and lastly desorption of product molecules [28]. The overall process may include a few reaction steps with a specific E_a for each step which is provided by thermalenergy. The thermal energy can be totally or partially supplied by light through photothermal conversion process which helps to reduce the overall reaction temperature required [4]. Moreover, photothermal heating can directly apply the heat at the reaction sites, which minimizes the heat loss and avoids excessive heat supply to the entire reaction system [7]. This localized heating can be controlled with precision and high conversion efficiency owing to the advancement in nanostructured photothermal materials. The reaction still follows the characteristic of traditional thermocatalysis at elevated temperatures, while the photothermal chemistry simply provides an alternative way to supply the thermal energy. Catalysts accelerate the reactions by decreasing the Gibbs energy of activation or modify the reaction pathways without affecting equilibrium and spontaneity of the reaction, thus the overall ΔG remains unchanged. The change of Gibbs free energy is always negative ($\Delta G < 0$) for thermochemical reaction from its initial state (reactants) to final state (products) [4].

2.2.3 *Photothermal chemistry in S-PTC*

In S-PTC, both light and heat are the driving forces for the reaction, achieving the synergetic effects between the photoinduced charges and heat activated conversion. Synergetic catalysis could make up for the disadvantages of pure photocatalysis, which lies in its relatively low efficiency and also helps to overcome the high energy-consumption problems of thermal catalysis. There are two scenarios: (1) Photocatalysis and thermocatalysis are realized separately with the first half-reaction activated by photocatalysis while the second half-reaction is driven by thermocatalysis [29]; and (2) photocatalysis and thermocatalysis occur simultaneously in the catalytic reaction with an outcome greater than the cumulative effect [30–32]. Such synergetic effects not only improve the catalytic activity but also bring enhancement in terms of selectivity of the desired products and stability of the catalyst. Moreover, with photocatalytic activation driving one of the reaction steps, it becomes viable to activate inactive materials or unfavourable reactions that are operating solely under thermal conditions. Consequently, a new catalytic pathway can be realized [33, 34].

2.3 Efficiency evaluation

To evaluate the efficiency of various photothermal catalysis systems for fuel production, both energy conversion efficiency and catalytic efficiency are used. For catalysis systems involving photochemistry-driven reactions, solar-to-fuel efficiency (STF) and apparent quantum efficiency (AQE) are used and can be calculated using Eqs. (1) and (2), respectively [21]

$$\text{STF}\ (\%) = \frac{\text{Chemical energy produced}}{\text{Solar energy input}} \times 100 = \frac{R_{\text{fuel}} \cdot \Delta G}{P \cdot A} \times 100 \quad (1)$$

where the R_{fuel} is the rate of production for a particular fuel, ΔG is the Gibbs free energy change for producing one mole of a particular fuel under standard conditions (237.2 kJ·mol^{-1}), P is the power density of solar irradiation intensity, and A is the area of the catalyst under irradiation.

$$\text{AQE}\ (\%) = \frac{\text{Number of reacted electrons}}{\text{Number of incident photons}} \times 100 = \frac{n \cdot R_{\text{fuel}}}{I} \times 100 \quad (2)$$

where n is the number of electrons required for the reaction, and I is the rate of incident photons.

Turnover frequency (TOF) is used to analyse the catalytic efficiency of the catalyst regardless of its composition and structure. TOF provides a reliable means for comparing the intrinsic activities of different catalysts and across various laboratories at a given set of reaction conditions. TOF can be calculated using Eq. (3) [35]

$$\text{TOF} = \frac{\text{The number of reactant converted or product produced}}{\text{The number of active sites} \times \text{reactiontime}} \quad (3)$$

where all the active sites on a catalyst are assumed to have the same activity, or one type of active site dominates the activity.

In PTC, both photochemical and thermochemical processes contribute to the overall efficiency of the reaction. In a free energy profile, the photochemical component helps to reduce the activation energy barrier of one or more steps throughout the catalytic process, while the thermochemical component increases the temperature at active sites to promote the probability of reactants overcoming the barrier based on Boltzmann distribution or promote the desorption of unwanted products from active sites [4, 6]. It is difficult to quantify the individual contribution from photochemistry and thermochemistry as the synergetic effect brings much higher efficiency than their sum. The differences in the reaction rates of various experiments can be used to estimate the contribution of light or heat. These include photothermal reaction rate with both irradiation and heating, photocatalytic rate with irradiation at room temperature, and thermocatalytic rate with heating in the dark [5]. This will be further discussed in Section 4.

3 Benefits of PTC

PTC has become an exciting and fast-growing field in recent years. The utilization of solar energy in photothermal catalytic reactions provides more sustainable ways for fuel production. The integration of photochemistry and thermochemistry elevates catalytic activities whilst keeping the operating conditions mild. They complement each other to enhance not only the catalytic activity, but also the selectivity for target products, and improve the durability and lifetime of the catalyst [36–39]. In this section,various benefits of photothermal chemistry in catalysis for fuel generation in terms of solar energy utilization, catalytic activity, selectivity of products, and stability of the catalyst are discussed.

3.1 Solar energy utilization

PTC promotes efficient solar energy utilization across the entire spectrum. In P-PTC, the high-energy photons are mainly used to generate the excited electronic state to induce a reaction via a photochemical process, while the low-energy visible and NIR photons are harnessed for heat to reduce the thermodynamic barrier of the reaction [40]. In T-PTC, the entire solar spectrum is harvested to provide thermal energy via a photothermal conversion process. In S-PTC, the thermal energy can interact with photoinduced carriers, and bring the synergetic effect of the thermocatalytic and photocatalytic processes [33].

In photochemistry-driven catalysis, the solar absorption is often limited by the bandgap of the semiconductor photocatalyst. P-PTC provides an efficient way to harvest visible to NIR solar spectrum for the photothermal heating effect to enhance the activity. Ozin's group demonstrated the photothermal heating effect with a 300 W Xe lamp focused to an intensity of ~ 20 kW·m^{-2} (~ 20 suns) for the reverse water gas shift (RWGS) reaction [41]. Under irradiation, the temperature of the $In_2O_{3-x}(OH)_y$/Si nanowire (SiNW) film reaches 150 °C and the CO production rate increases from 0.8 to 22.0 μmol·g^{-1}·h^{-1}. With the nanostructured SiNW photothermal support, broadband solar irradiance can be used to drive an efficient CO_2 reduction reaction (Fig. 3(a)). Ho's group developed a core–shell structured SiO_2/Ag@TiO_2 photocatalyst with the TiO_2 for photocatalytic electron–hole pair generation, while lower-energy photons are captured by the SiO_2/Ag photothermal core for heat generation (Fig. 3(b)) [42]. The core–shell nanocomposite obtained a photothermal enhancement of ~ 95% under one sun (1 kW·m^{-2}) compared with UV irradiation alone. The maximum hydrogen generation rate of 13.3 mmol·g^{-1}·h^{-1} under natural sunlight demonstrated an experimental proof for broadband photocatalytic hydrogen generation.

In traditional thermochemistry-driven catalysis, the harsh condition with intensive energy input is usually prescribed. In both T-PTC and S-PTC, light could assist to enhance the local temperature, thus decreasing the external heat intake, or totally replacing the heat source via high flux light intensity to drive the thermal catalysis reactions. Han et al. integrated Pt/black TiO_2 catalyst with the light-diffuse-reflection surface of SiO_2 substrate to assist methane reformation. Without irradiation, the typical thermocatalytic reaction occurred at 550 °C. Upon AM 1.5 sunlight irradiation, the reaction manifested at 350 °C, signifying the reduction of the activation temperature by 200 °C. Moreover, the yields of H_2 and CO at 650 °C increased from 9 and 99 mmol·h^{-1}·g^{-1} in the dark to 129 and 370 mmol·h^{-1}·g^{-1} under visible light irradiation, respectively [43]. These findings indicate the promising solar energy utilization in the field of solar-assisted thermocatalysis. Moreover, by incorporating nanomaterials with stronger light absorption abilities, the thermocatalytic reaction can be driven completely by solar energy. Li et al. demonstrated completely solar-driven thermocatalytic steam reforming of ethanol and methanol with Ti_2O_3 and Bi_2Te_3/Cu as the photothermal materials respectively, and obtained corresponding hydrogen production rates of 20.7 and 310 mmol·g^{-1}·h^{-1} under 1 sun irradiation [44, 45]. Ye et al. investigated the photothermal effect of Group VIII metal nanoparticles (NPs) supported on γ-Al_2O_3 for CO_2 conversion. Under continuous irradiation, Group VIII catalysts reached an equilibrium temperature of 300–400 °C, which is almost 200 °C higher than that of γ-Al_2O_3 support (Fig. 3(c)) [46]. Specifically, the CO_2 reaction rate of Ru can reach up to 18.16 mol·h^{-1}·g^{-1} with a conversion efficiency of 95% and CH_4 selectivity of 99%. It identifies the great potential for the development of light-driven thermocatalysis and illustrates the feasibility of full spectrum utilization.

In S-PTC, light does not only contribute to heating, but also bring other synergetic effects. For example, hot carriers can be generated upon irradiation in plasmonic materials, and the hot electrons can be injected into the adsorbates through direct or indirect hot carrier transfer mechanisms [47–49]. With the

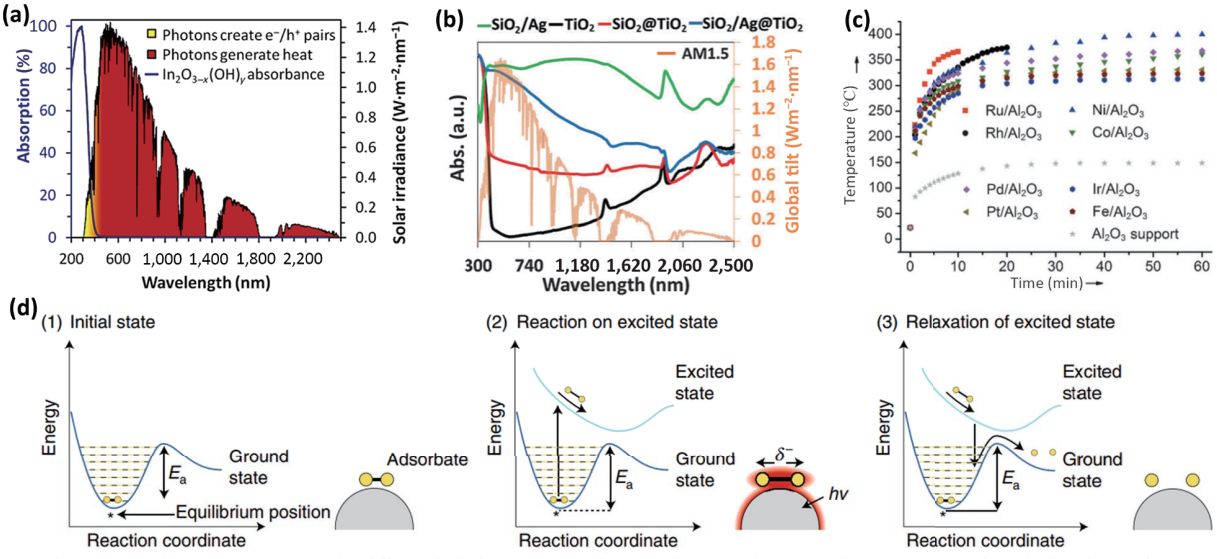

Figure 3 Solar energy utilization in PTC. (a) The different light harvesting mechanisms between photons with energy greater than the band gap of $In_2O_{3-x}(OH)_y$, which have the ability to create an electron/hole pair within the nanoparticles (yellow), and photons with energy less than the band gap of $In_2O_{3-x}(OH)_y$, which are absorbed and converted into heat energy within the SiNW support (red). Reproduced with permission from Ref. [41], © American Chemical Society 2016. (b) Calculated absorption spectra of various samples and the spectral solar irradiance (AM 1.5). Reproduced with permission from Ref. [42], © The Royal Society of Chemistry 2016. (c) Monitoring of the catalyst temperature via photoirradiation induced thermal effect. Reproduced with permission from Ref. [46], © WILEY-VCH Verlag GmbH & Co. KGaA, Weinheim 2014. (d) Schematic of the desorption induced by electronic transitions mechanism for a dissociation reaction on a photoexcited plasmonic metal. (1) The adsorbate initially sits at the equilibrium position on its ground-state potential energy surface, requiring activation energy E_a to dissociate. (2) Photoexcitation of the plasmonic nanoparticle deposits plasmon energy into the adsorbate and elevates it to an excited potential energy surface. The adsorbate then moves along the excited potential energy surface, gaining kinetic energy and possibly reacting in the excited state. (3) If the adsorbate does not react in the excited state, it decays back down to the ground-state potential energy surface in a vibrationally excited state effectively lowering the barrier for dissociation. Reproduced with permission from Ref. [50], © Aslam, U. et al. 2018.

assistance of hot carriers, the adsorption of reactant molecules, the activation of chemical bonds, and the conversion of intermediates will be promoted, which facilitates the catalytic activity (Fig. 3(d)) [50]. In addition, oxygen vacancies in semiconductor materials introduce electrons trapped in shallow energy states, and these electrons can be released upon light irradiation and enhance the surface reduction reaction rate. This approach fully utilizes the solar spectrum in terms of both heat and light, thus further enhances the solar-to-fuel conversion efficiency.

3.2 Catalytic activity

The synergetic effects from photochemical and thermochemical processes bring a much higher catalytic activity than a simple combination of them. Although this effect has been observed by various research groups, the in-depth investigation is still at its early stage. In this section, primary effects on boosting the catalytic activity are identified and discussed, including providing localized heating at the reaction sites, reducing the apparent activation energy, promoting the rate-determining step, as well as increasing carrier mobility and mass transfer.

3.2.1 Global and localized heating

The heat involved in PTC is commonly from two sources, thermal energy from irradiation via the photothermal conversion process, or external heating by an electric heater. In the global heating system, thermal energy is often supplied by external heating sources causing a bulk increase in the temperature of the whole reaction system. This is commonly applied in traditional thermocatalytic systems. On the other hand, localized heating is obtained by a nanostructured solar absorber converting the photon energy into heat, subsequently released at nanoscale premises [24, 51]. In the case when high intensity or concentrated light source is used, global heating may also be initiated.

In the global heating system, external heating sources have been adopted to study the temperature effect on the performance of PTC. In photochemistry-driven catalysis, the temperature rise is often viewed as an undesirable effect on reaction rate due to the promotion of charge recombination especially when an efficient charge transfer path is inaccessible. However, the temperature effect has been recently demonstrated with beneficial results in P-PTC. Ho's group [52] demonstrated the heating effect on photocatalytic hydrogen generation using TiO_2 nanotubes loaded with CuO nanoparticles. The AQE increases from 10.3% to 66.9% when the temperature rises from 25 to 90 °C. Ozin's group [53] studied the temperature effect on $In_2O_{3-x}(OH)_y$ nanoparticle film in the gas-phase photocatalytic conversion of CO_2 in the presence of H_2 to generate CO. There is an increase in photocatalytic CO production with reaction temperature. The maximum rate of 0.25 $\mu mol \cdot g_{cat}^{-1} \cdot h^{-1}$ is achieved at 150 °C under simulated solar illumination intensities of 2,200 $W \cdot m^{-2}$. Li et al. developed Au/N-doped TiO_2/MgO (111) nanocatalyst with its photocatalytic activity highly dependent on applied temperatures [54]. The results reveal that the dissociation of H^+ and OH^- from water becomes more favorable at higher temperatures and peaked at around 270 °C.

Besides external heating, global heating can also be derived from high intensity or concentrated light irradiation. Liu's group demonstrated the heating effect of photocatalytic CO_2 reduction. The production rates of CO and CH_4 are enhanced by 13.2 and 111.3 times respectively with TiO_{2-x}/CoO_x catalyst when the temperature increases from 298 to 393 K using only light (150 W UV lamp) to supply the heat [55]. In Chen et al.'s work, the temperature of CoFe-650 catalyst could stabilize at 310 °C after light irradiation for 30 min, driving CO_2 hydrogenation reaction (Fig. 4(a)) [56]. Noticeably, the CO_2 conversion administered by light-induced heating was almost similar to thermocatalysis, indicating the T-PTC mechanism that the photothermal pathway embraces the thermocatalytic rather than the photocatalytic mechanism (Fig. 4(b)). Moreover, global heating can also be supplied by a combination of external heating and irradiation. Li's group prepared Pt-supported Si-modified CeO_2 catalyst for

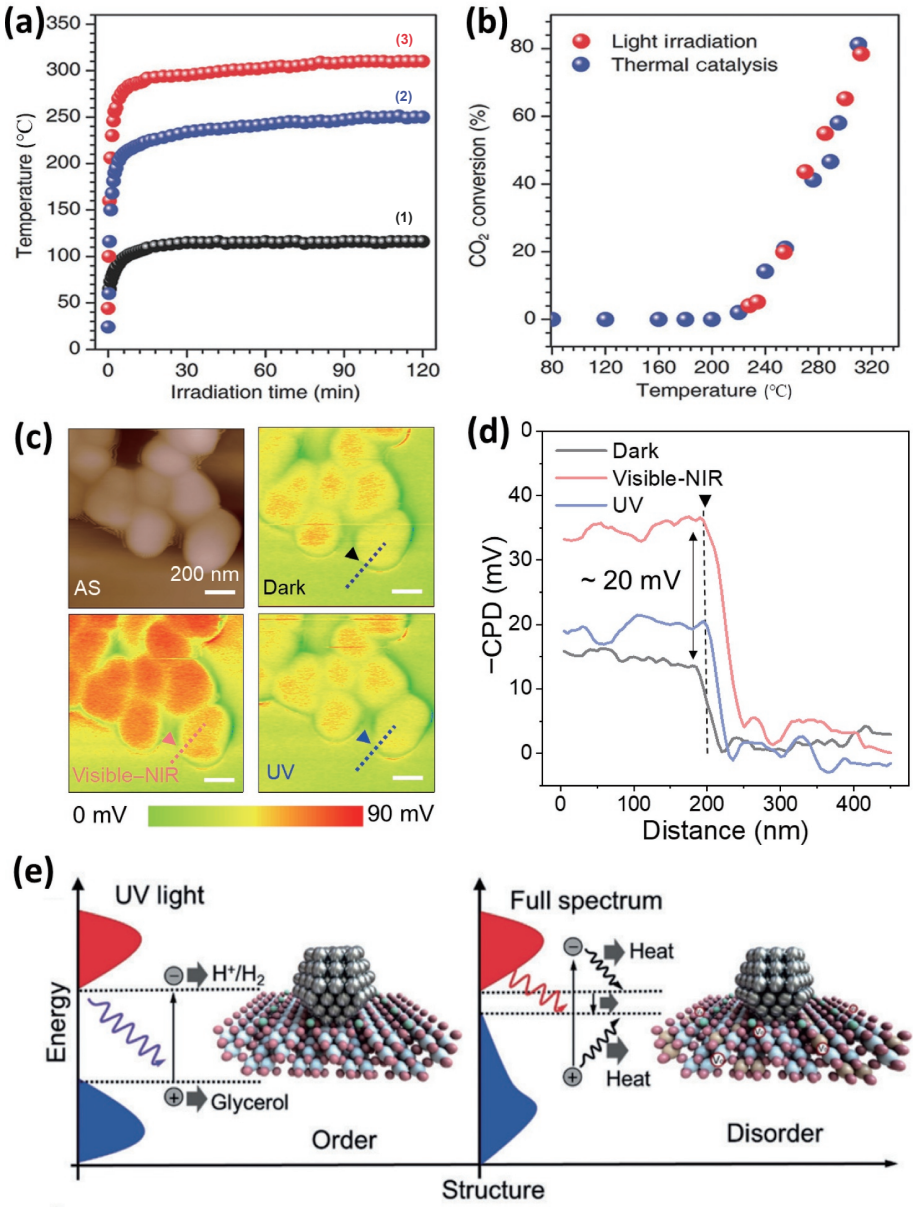

Figure 4 Global and localized heating in PTC. (a) Temperature profiles for: (1) reactor without any catalyst under UV–vis irradiation, (2) CoFe-650 under visible irradiation, and (3) CoFe-650 upon UV–vis irradiation. (b) Comparison of CO_2 conversion for CoFe-650 under photothermal heating (UV–vis irradiation) and direct thermal heating (no UV–vis irradiation). Reproduced with permission from Ref. [56], © WILEY-VCH Verlag GmbH & Co. KGaA, Weinheim 2017. (c) Topography and the inverse contact potential difference (–CPD) of $Ag@SiO_2$ (AS), and (d) line profiles of –CPD along lines marked in (c) under various light source illumination. Reproduced with permission from Ref. [62], © Wiley-VCH GmbH 2021. (e) Schematic illustration of the band energies and the light absorption properties of HNb_3O_8. Reproduced with permission from Ref. [64], © WILEY-VCH Verlag GmbH & Co. KGaA, Weinheim 2019.

photocatalytic and thermocatalytic coupling effects on dry reforming of methane [57]. The temperature of the catalyst can reach up to 420 °C under the concentrated solar simulator's irradiation (the equivalent of 30 suns) and when external heat was furnished to further increase the reaction temperature to 600 °C, the photothermal H_2 and CO production rates were 5 and 2 times higher than those in dark at the same temperature.

In the localized heating system, heat is directed at the reaction sites, which minimizes the heat loss and avoids the excessive heat supply to the entire reaction system to warrant high photothermal conversion efficiency. This localized heating can be controlled with precision owing to the advancements in nanostructured solar absorbers. Based on different interaction mechanisms of electromagnetic radiation with matter, localized heating can be realized by electron oscillation in plasmonic materials, non-radiative relaxation in semiconductors, and lattice vibration in organic materials [23]. With the localized heating in place, the enhancement is often greater than that at the same reaction temperature through external heating [58–61]. Ho's group designed $Ag@SiO_2@TiO_2$ nanosheets with the $Ag@SiO_2$ as the heating core for localized plasmonic photothermal effect and showed an enhancement of ~ 170% for hydrogen generation based on P-PTC [62]. Experiments have proven the localized heating effect by keeping the reaction solution at a fixed temperature of 50 °C whilst hydrogen production rate was observed to increase by ~ 37.5% with visible and NIR light irradiation. This enhancement is ascribed to the localized plasmonic heating effect of $Ag@SiO_2$. This effect has also been examined with the inverse contact potential difference (–CPD) of $Ag@SiO_2$ (AS) in dark, illuminated under vis–NIR or UV light (Figs. 4(c) and 4(d)). The results validate that more hot electrons are generated under vis–NIR light, resulting in the upward shift of the Fermi level and a decrease in work function, which is favorable for the localized photothermal effect. At present, defects and/or

vacancy-rich materials also exhibit excellent light absorption capacity and realize efficient photothermal conversion. Ozin's group reduced pale yellow In_2O_3 to black oxygen-vacancies In_2O_{3-x} for S-PTC of RWGS reaction [63]. Compared to the low CO production rate of 19.64 μmol·g^{-1}·h^{-1} over yellow In_2O_3, the black In_2O_{3-x}/In_2O_3 can reach up to 23,882.75 μmol·g^{-1}·h^{-1} and 100% selectivity towards CO. The oxygen vacancies enable enhanced optical absorption across the solar spectrum to give rise to confined heating for thermal conversion of CO_2 to CO, while the photogenerated electron–hole pairs can be separated across the interface between In_2O_3 and In_2O_{3-x}, thereby promoting the photochemical conversion of CO_2. Ho's group investigated the photothermal effect of *in-situ* synthetically immobilized lattice distortions in monolayer HNb_3O_8 for hydrogen generation in P-PTC [64]. The incorporated lattice disorders generate new energy states with small band gap that induce full solar spectrum absorption with ca. 80% average absorbance (Fig. 4(e)). This results in the photothermal effect localized at the catalyst-reactant complexes' proximity, and an enhancement of 272% hydrogen generation.

Localized heating can transpire without the increase of temperature for the overall reaction system, or even the entire catalyst. Ozin's group formulated active palladium "nanoheaters" on Nb_2O_5 nanorods to achieve a local temperature that is high enough to drive the catalytic hydrogenation of CO_2 [65]. As the heating is spatially confined at the interface, the sintering phenomenon, which only occurs with the macroscopic heating of the entire nanostructured catalyst, is not observed here. However, in many cases, global and localized heating co-exists when multiple or broadband light-absorbing nanomaterials are used. In the previously mentioned examples of localized heating from Ho's group [62, 64], the increase in the reaction solution temperature has also been observed in this P-PTC for hydrogen generation.

In summary, global heating is used to enhance the performance by increasing products formation rate or improving mass transfer in P-PTC [6]. In the T-PTC reaction, global heating provides the thermal energy to drive the thermochemical reaction, while the activation temperatures are comparable with either photo heating or external heating. In the presence of localized heating, heat can be confined at the reaction sites without scattering to the surrounding, thus the overall temperature required for the thermochemical-driven reaction can be reduced. Both thermal and other non-thermal effects from irradiation could exist in S-PTC, the synergetic effects often bring higher reaction rates than the sum of individual reactions. The localized heating can be tuned by the composition, size, shape, and chemical environment of the nanostructured solar absorber. Moreover, the high controllability of localized heating in terms of site, magnitude, and duration of heat generation makes it more effective for targeted reactions in all three types of photothermal catalysis for fuel generation. The fast photothermal heating and cooling process is also useful for on-demand production.

3.2.2 *Improving mass transfer*

The mass transfer process of the reactant and product molecules will be enhanced by thermal energy, resulting in a positive effect on the catalytic reaction rate [66]. Increasing temperature favors the diffusion of molecules in the reactor, giving rise to increased interaction between energetic carriers and reactants at the reaction sites. This is certainly beneficial for the activation of chemical bonds and thus enhances the catalytic performances [67]. Li et al. designed ultrathin porous g-C_3N_4 nanosheets decorated with AuCu alloy nanoparticles for S-PTC CO_2 reduction to ethanol [68]. The increase in temperature promotes the thermodynamics of the reactant molecules, which leads to improved dimerization of *CO and the formation of C–C coupling. Together with more active sites, better charge transfer, and enhanced adsorption of CO_2, the AuCu/g-C_3N_4 catalyst obtained 4.2- and 7.6-times higher production rate in photothermocatalysis than that in photocatalytic and thermocatalytic reaction, respectively. Liu et al. developed the WN-WO_3 Z-scheme heterostructure for water-based CO_2 conversion [69]. The heterostructure is able to absorb a wide solar spectrum and can reach 154 °C in 10 s under simulated solar irradiation. The UV–vis light is used for photocatalytic reaction while the infrared (IR) light is exploited for creating a local photothermal effect. Based on the temperature-dependent kinetic experiment on the photocatalytic CO_2 conversion, the local photothermal effect is beneficial for accelerating the reactant adsorption–desorption process and charge carrier transportation, thus enhancing the conversion efficiency with total consumed electron number (TCEN) for CO_2 conversion to be 355.2 μmol·g^{-1}·h^{-1}.

3.2.3 *Facilitating reaction kinetics*

The photothermal condition not only improves the mass transfer, but also reduces the activation energy. Ghuman et al. experimentally observed that the activation energy of the gas-phase reaction of CO_2 with H_2 was reduced by about 20 kJ·mol^{-1} using a defective $In_2O_{3-x}(OH)_y$ under irradiation compared to the thermochemical reaction in the dark [70]. The reaction rate is improved by four times. Later, they found that the population of low-lying energy states associated with the surface enhances the Lewis acidic and Lewis basic character besides being more active in the excited states compared to the ground states (Fig. 5(a)) [71]. Yu et al. also found that at elevated temperature, the photocatalytic CO_2 reduction rate of solution-plasma-processed TiO_2 with rich oxygen vacancies increases 300 times [72]. This could be due to the release of the electrons trapped in shallow energy states at high temperature (Fig. 5(b)). These freed electrons accelerate the surface reduction of the adsorbed species, thus enhancing the reaction rate. Jiang et al. confined Pd_3Cu nanoparticles into UiO-66 scaffold for light-assisted CO_2 hydrogenation to methanol [73]. Besides the thermal effect, the photoinduced electrons produced by UiO-66 metal-organic framework (MOF) transferred to antibonding orbitals of CO_2* and promoted the activation of CO_2 (Fig. 5(c)). Moreover, the close proximity between CO_2 and H_2 activation sites on Pd_3Cu NPs and defective Zr–oxo clusters respectively, greatly facilitates their interaction and conversion. As a result, the MOF-confined Pd_3Cu NPs catalyst exhibited a remarkable improved methanol production rate of 340 μmol·g^{-1}·h^{-1} under photothermal conditions.

Moreover, the photon-induced high energy hot carriers from plasmonic materials can also introduce extra photoactivation mechanisms into traditional thermochemistry-driven catalytic systems and activate the reactant molecules to participate in reactions. Ye et al. found that Au inactive in the dry reforming of methane (DRM) reaction, could serve as the plasmonic promoter with Rh/SBA-15 as the catalyst [74]. The electromagnetic field simulations showed strong localized electric-field enhancement with the interparticle coupling between Au NPs and Rh NPs. The photoinduced highly energetic electrons by localized surface plasmon resonance (LSPR) of Au promote the polarization and activation of CO_2 and CH_4. The desired catalysts showed enhanced catalytic performance in DRM under visible light irradiation by 1.7 times and the CO_2 conversion rate increased from 2,100 to 3,600 μmol·g^{-1}·s^{-1}. Jia and co-authors also investigated Au/CeO_2 catalysts for driving RWGS under pure thermal and photo-thermal conditions [75]. Based on the *in-situ* diffuse reflectance infrared Fourier transform spectroscopy (DRIFTS) results, it was proposed that Au played a decisive role in

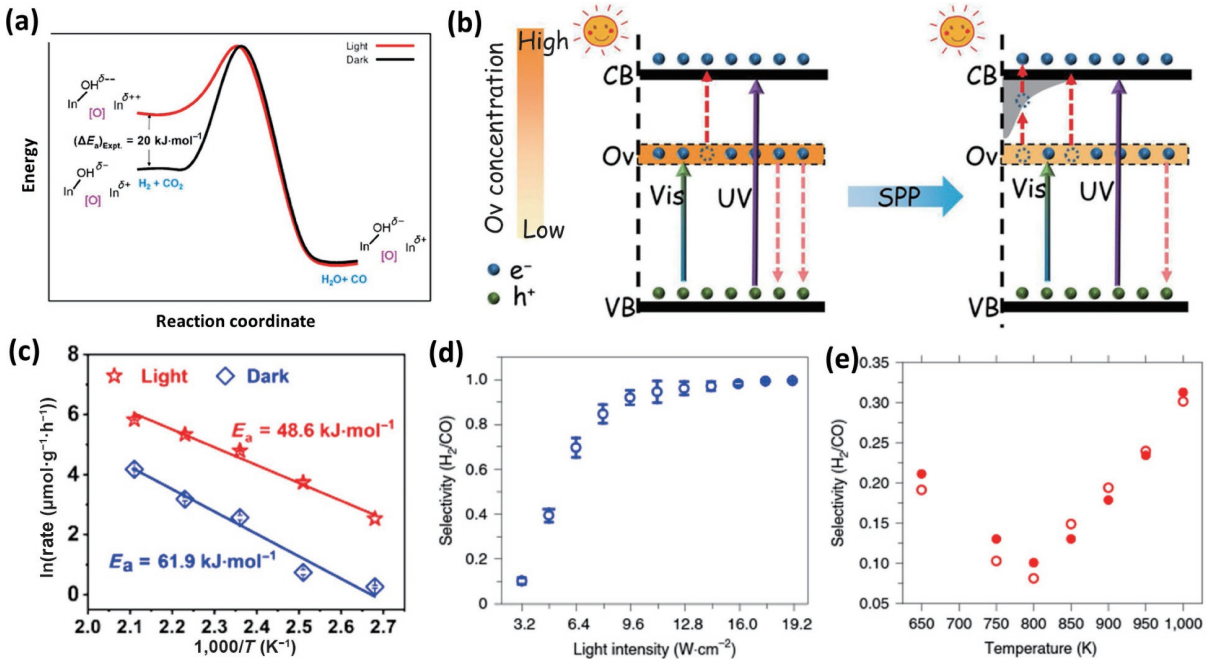

Figure 5 Photothermal chemistry for facilitating reaction kinetics and selectivity. (a) Schematic illustration of the origin of the difference in the experimental activation energy $(\Delta E_a)_{Expt.}$ for the reverse water gas shift reaction $CO_2 + H_2 \rightarrow CO + H_2O$ involving the ground state surface frustrated Lewis pairs in the dark and excited-state surface frustrated Lewis pairs in the light. Reproduced with permission from Ref. [71], © American Chemical Society 2016. (b) Schematic illustration of the electron–hole separation mechanism for samples before and after solution plasma processing during photocatalysis driven by UV and visible light irradiation. Reproduced with permission from Ref. [72], © WILEY-VCH Verlag GmbH & Co. KGaA, Weinheim 2020. (c) Arrhenius plots of CH_3OH yield under dark and light conditions. Reproduced with permission from Ref. [73], © Wiley-VCH GmbH 2021. (d) Light intensity dependence of selectivity in photocatalysis. Error bars represent the standard deviation (σ_{std}) of measurements of three different batches of sample. (e) Temperature dependence of selectivity in thermocatalysis. Filled and unfilled circles represent the measurements of two different batches. Reproduced with permission from Ref. [80], © Zhou, L. N. et al. 2020.

high photothermal CO_2 conversion ability, as the hot electrons from Au would contribute to the dissociation of absorbed H_2 on the surface and facilitate CO_2 hydrogenation to CO. Similar results have been demonstrated with Pd_xAu_y/Al_2O_3 [76] and Pt-Au/SiO_2 [77] catalysts, and the hot electrons generated from excited plasmonic NPs facilitate the activation of the reactants and/or intermediate species, resulting in enhanced light-assisted reaction rates compared with the thermocatalytic reaction. The hot energy electrons may take part in the activation of the reactant or intermediate species at an earlier stage before the rate-determining step. In this case, some photochemical process contributes to the reaction rate, but it may not necessarily result in lowering the activation barrier of reaction.

In addition, when photocatalytic activation is driving one of the reaction steps in S-PTC, inactive materials or unfavourable reactions operating under thermal conditions can be activated to induce new catalytic pathways [78, 79]. Zhang et al. proposed a novel photo-thermochemical cycle that photochemistry and thermochemistry occur sequentially for CO_2 decomposition via solar energy [29]. The overall cycle can be divided into two steps. In the first step, it is the photochemical process that utilizes ultraviolet light to reduce TiO_2 to TiO_{2-x} and forms surface photo-induced V_o. In the second step, the thermochemical cycle will set in, and the active V_o adsorbs CO_2 molecule and forms a stable CO_2 state. When subjected to heating, the transitional balance state is perturbed and electrons transfer from Ti^{3+} to CO_2 follows, which breaks the chemical bonds to produce CO and oxidize TiO_{2-x} to TiO_2. The photochemical process replaces the first step of the thermochemical cycle with high temperature (> 1,273 K), and provides a novel cycle for dissociation of CO_2.

3.3 Selectivity of products

When photogenerated high energy electrons are injected into the surface of intermediate species, it may change the electronic properties of active sites or lead to surface construction. Accordingly, this may potentially favor an alternate pathway and change the selectivity of target products that cannot be realized in thermocatalytic processes alone. Halas et al. designed a Cu-Ru antenna-reactor plasmonic photocatalyst for low temperature light-driven DRM [80]. $Cu_{19.8}Ru_{0.2}$ catalyst demonstrated an optimal DRM photothermal performance with a turnover frequency of 34 $mol_{H_2}·mol_{Ru}^{-1}·s^{-1}$ under light irradiation without thermal heating. Noticeably, the selectivity of photocatalytic DRM increased with light intensity while the thermal selectivity showed an obvious V-shape trend over temperature (Figs. 5(d) and 5(e)). This stark contrast confirmed the hot-carrier is the dominant mechanism rather than general light conversion to heat. Based on the mechanistic study, it was revealed that the plasmonic Cu could transfer hot electrons to the surface of Ru, which was the main active sites for CH_4 dehydrogenation to prevent the side reactions of RWGS and coke formation, thus shifting the chemical equilibria toward a higher yield of target products. Ozin et al. systematically tailored 5 to 20 nm Pd "nanoheaters" supported on Nb_2O_5 nanorods for CO_2 hydrogenation reaction and showed an increasing trend in light absorption with Pd particle size [81]. Upon irradiation, Pd efficiently converts the absorbed light into heat that causes an elevated local temperature of the Nb_2O_5 support and drives the reaction. The CH_4/CO selectivity is positively correlated with the light intensity, thus indicates the photothermal capability of the sample affects the selectivity. Moreover, as the size of the Pd nanocrystal with different surface chemistry changes the adsorption strength of reactants, intermediates, and products, it also affects the selectivity. For large Pd nanocrystals, the methanation process ($CO_2 + 4H_2 \rightarrow CH_4 + 2H_2O$) was favoured and the production rate of CO and CH_4 can reach up to 0.75 and 0.11 $mol·h^{-1}·g^{-1}$ while small Pd facilitated RWGS and 99.5% selectivity towards CO was observed. The reaction selectivity involves reactants, adsorbates on the surface,

intermediates, final product, and adsorption–desorption process in the overall reaction process. Any change in these species would shift the reaction equilibrium towards an alternate mechanism. Therefore, the selectivity typically does not occur separately and may be accompanied by photoactivation and reduction of reaction barrier effects.

3.4 Stability of the catalyst

As mentioned above, the basic catalysis reaction generally includes adsorption and activation of reactants, bond dissociation and conversion of intermediates, and desorption of products. From the perspective of activity and selectivity, thermal and light energy can contribute to the reaction by activating specific chemical bonds of reactants or intermediates, thus reduce the reaction barrier or modify the reaction pathway to the desired direction. Alternatively, the heat or photoinduced electrons can also accelerate the desorption of unwanted species from the surface of catalysts, which benefits the activity and stability of active components. This was demonstrated by Mateo et al. in their study about NiO/Ni supported on graphene for efficient photocatalytic CO_2 methanation [82]. It was evidenced that H_2O desorption was one critical factor to determine the activity and that was why the system required heating. The desorption of water product would deactivate the catalyst and thus in the continuous flow system, NiO/Ni-graphene showed a lower CH_4 production rate than that in the batch reactor. Pan et al. found that the light illumination on MgO/Pt/Zn-CeO_2 for the dry reforming process possesses outstanding stability without obvious decay at 600 °C for 20 h testing, while severe deactivation is observed when the reaction is performed in the dark at the same temperature [83]. The enhanced stability is attributed to the *in-situ* generation of oxygen vacancy on CeO_2 by photoinduced electrons, which balances the consumption and generation of oxygen vacancies as CO_2 activation sites. Moreover, the quick deactivation of Ni-based catalyst due to concomitant side-reaction of carbon deposition is a great challenge for stable thermo-activation. Zhang et al. found that the photoactivation of Ni-La_2O_3/SiO_2 for CO_2 reduction by CH_4 restrains CO disproportionation which is a major side-reaction for carbon deposition [84]. The rate of carbon deposition reduces from 3.31×10^{-2} to 1.74×10^{-2} $g \cdot g^{-1} \cdot h^{-1}$ under UV–vis–IR irradiation.

4 Methodologies

It is important to distinguish the photochemical and thermochemical contributions in the PTC process in order to understand the mechanisms of the catalytic reactions. This will not only help the rational design of catalyst, but also optimize the reaction condition for the PTC [33]. However, it is particularly challenging to differentiate them, especially in the case of S-PTC when the two mechanisms occur concurrently, and photon and thermal-induced effects take place simultaneously [13]. In this section, we have summarized various strategies, including experimental designs, thermometry characterization techniques, and computational studies, that help to identify and quantify the various effects of PTC catalysis.

4.1 Experimental designs

The photochemical and thermochemical contributions can be isolated to a certain extent by performing the experiments under various prescribed settings. These entail photocatalytic setting with light irradiation at room temperature, thermocatalytic setting at a specific temperature in the dark, and photothermal setting that holds the reaction at a specific temperature under light irradiation [5, 85]. Depending on the heating sources, external physical heating, or light irradiation, different temperatures or light intensities and wavelengths can be tuned respectively to further examine the enhancement of the catalytic reaction [86].

In P-PTC, no activity is observed under the thermocatalytic setting, the difference between photothermal and photocatalytic settings reveals the enhancement from thermal contribution. Ho's group designed photothermal catalytic gel consisting of TiO_2/Ag nanofibers (NFs) with the Ag nanoparticles for localized plasmonic photothermal effect and showed photothermal enhancement of ~ 395% for hydrogen production [87]. Experiments were conducted to isolate the localized heating effect through controlled reaction solution temperature at 35 °C. The hydrogen production rate increases by ~ 107% when visible and NIR light is introduced while the reactor is maintained at the same temperature (Fig. 6(a)). This enhancement is ascribed to the localized plasmonic photothermal effect where the heat generated by the Ag nanoparticle is mainly confined at the nanoscale around the active sites. Moreover, the hydrogen production rate has been tested using various monochromatic light sources in the visible and NIR ranges. The results reveal that the hydrogen production rate conforms with the LSPR absorption of Ag with the maximum rate at 450 and 505 nm which are within the resonance band of Ag nanoparticles (Fig. 6(b)).

In T-PTC, the photocatalytic setting cannot activate the catalytic reaction. The increment of activity under the photothermal setting compared with the thermocatalytic setting indicates the enhancement from light contribution. Huang et al. demonstrated that Ni with silica modified cluster showed no activity under light irradiation below 400 °C. Only when the temperature was above 400 °C, the activity was considerably improved under focused irradiation, indicating the solar light-driven thermocatalysis mechanism [88].

In S-PTC, experiments under all three conditions should be carried out. In this case, it is quite difficult to decouple and quantify the two different mechanisms, because the synergetic effects between them often reveal higher activity than the sum of their individual activities. Li et al. introduced an indirect irradiation technique to distinguish the thermal and non-thermal effects on photocatalytic CO_2 methanation [89]. By introducing an inactive layer of Ti_2O_3 on the top of the Rh/TiO_2 catalyst, identical thermal profiles of the Rh/TiO_2 catalyst compared with direct irradiation have been obtained with complete elimination of hot carrier contribution, thus isolating the nonthermal effect from light irradiation on the photocatalytic activity (Figs. 6(c) and 6(d)). In S-PTC catalysis, the individual photoinduced charge carriers and heat activation contribute to the reaction simultaneously. From the above section on the discussion of the effects of photothermal, it can be concluded that photoinduced carriers may participate in the overall catalytic process in various steps, such as activating the reactant molecules, initiating an alternate mechanism, changing the selectivity of target products, and enabling the desorption of unwanted species from the surface of catalysts. It is significant to evaluate the contribution of photoinduced carriers from photochemistry aspects. There are several experimental techniques that can differentiate the contribution of photoinduced carriers from the photothermal heat effects. Firstly, high-pass cut-off filters are used with variable Xe lamp light intensity to compare the differences in activities under photothermal and thermal conditions. When the catalytic reaction is induced by photo-generated electrons, the production rate will exhibit a linear activity with the photon flux and single wavelength. In Robatjazi's work, the CO production rates of Al@Cu_2O showed a positive trend with increasing visible light intensity [90]. The external quantum efficiencies (EQE) increase with incident photon flux, indicating the characteristic of plasmon-induced charge-carrier driven photocatalysis (Figs. 6(e) and 6(f)).

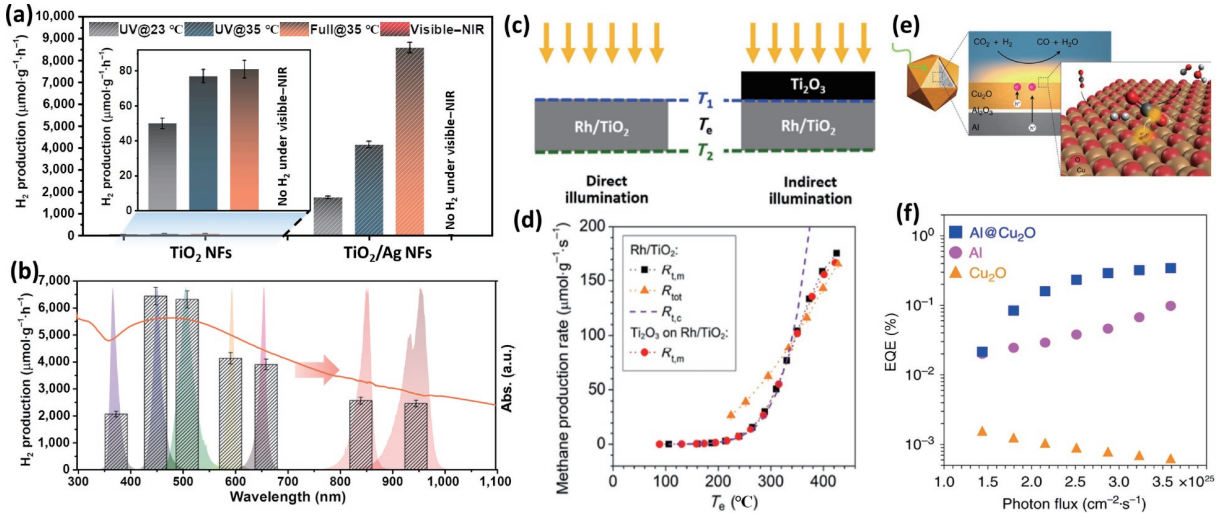

Figure 6 Differentiate the photochemical and thermochemical contributions through experimental designs. (a) Hydrogen generation rates of TiO_2 and TiO_2/Ag NFs under UV, visible–NIR, and full spectrum irradiation at various environment temperatures. The inset is the zoomed figure of the hydrogen generation rates of TiO_2 NFs under various conditions. (b) The photocatalytic hydrogen generation rate of the TiO_2/Ag NFs under different monochromatic light irradiation conditions, and its corresponding absorption spectrum. Reproduced with permission from Ref. [87], © WILEY-VCH Verlag GmbH & Co. KGaA, Weinheim 2020. (c) Schematic representation of photocatalytic reactions under direct and indirect illumination. (d) CH_4 production rates shown as a function of equivalent temperature (T_e). For the uncovered Rh/TiO_2 catalyst, the measured rate under dark thermal conditions (black squares) and under direct illumination with additional external heating (orange triangles) are plotted. For the covered catalyst, the measured rate under dark thermal conditions (red circles) is shown. The calculated thermal CH_4 production rate (purple dashed lines) as a function of T_e is also shown in the figure. Reproduced with permission from Ref. [89], © Tsinghua University Press and Springer-Verlag GmbH Germany, part of Springer Nature 2019. (e) Schematic of plasmon-induced carrier-driven RWGS on Al@Cu_2O. (f) The apparent external quantum efficiency was calculated from measured reaction rates of various samples and plotted against photon flux. Reproduced with permission from Ref. [90], © Robatjazi, H. et al. 2017.

Secondly, the selectivity of the target products under both photothermal (light-induced) and purely thermal conditions is to be examined. The formation of CO and CH_4 in the thermal process completely depended on the reaction temperature, while it showed a higher selectivity towards CO in the light-induced RWGS reaction. This stark contrast implied the participation of hot carriers from the perspective of photochemistry instead of photothermal heating.

4.2 Thermometry characterizations

In PTC catalysis, photothermal conversion to heat and photoinduced high energy electrons co-exist to synergistically promote the surface chemical catalysis reactions. To reveal the thermodynamics and kinetics of the photothermal mechanism, it is essential to measure the temperature of the system and at the surface active sites. The lifetime (fs) of hot carriers is considerably short compared to the chemical reactions time level (ps). Therefore, hot carriers contribute to limited adsorption and activation of photothermal reactions from photochemistry. The remaining photoinduced electrons and holes will recombine and release energy through heat dissipation, acting as an additional energy input to assist or totally drive the photothermal reactions. Since the thermodynamics and mechanism are determined by the temperature, it is necessary to develop accurate temperature measurement technology. Primitively, a thermocouple is directly contacted to the catalysts surface and provides intuitional information about the catalyst temperature. For example, Cai et al. tested the surface temperatures of different Ni@SiO_2 films with a direct contacting thermocouple and found the core–shell Ni@SiO_2 sample had the highest stabilized surface temperature [91]. However, thermocouple can only roughly reflect the temperature change and may not accurately tell the true temperature of the overall surface on the catalysts. IR camera is another common instrument that is widely used for temperature measurement. Li et al. measured the spatial temperature images of Ni/Y_2O_3 photothermal catalyst under 1 sun by IR camera. IR cameras present the surface temperature of the catalyst but not the actual temperature at the active sites due to their limited resolution and penetration ability [92]. Especially with the manifestation of localized heating, it is difficult to measure the accurate temperature at the nanoscale. Cai et al. estimated the microscopic local temperatures achieved by Ni@p-SiO_2 based on equilibrium constants of the RWGS reaction and the Sabatier reaction [93]. Some recently advanced nanoscale thermometry such as scanning thermal microscopy equipped with nanoscale probe tips (Figs. 7(a)–7(c)) [94], scanning transmission electron microscopy with electron energy loss spectroscopy [95], anti-Stokes thermometry from a single hyperspectral photoluminescence confocal image (Figs. 7(d)–7(f)) [96], *in-situ* X-ray absorption spectroscopy [97], and Raman spectroscopy [98] can provide information about the temperature with nanometer-scale resolution. It was found that Raman bands of metal oxides would shift to a lower frequency along with high temperature due to the thermal expansion of lattice and changes in the vibrational energy [99]. Based on the Raman results, the temperature of Pd@Nb_2O_5 was estimated to be 777 K while pure Nb_2O_5 was only 368 K for photothermal reverse water gas shift reactions (Figs. 7(g)–7(i)) [81].

4.3 Computational studies

Besides experimental and characterization methods, computational study is another useful technique to reveal the mechanisms in PTC catalysis. Three-dimensional finite-difference time-domain (3D-FDTD) can be adopted to study the interaction between light and catalyst, while the density functional theory (DFT) calculations can be used to investigate the electronic structures or adsorbed species and intermediates on the surface active sites. Xu et al. performed 3D-FDTD simulations to study the optical absorption and calculate the spatial electric-field distribution of palladium-nanoparticle-loaded TiO_2 as a function of the incident wavelength of light (Fig. 8(a)) [78]. The calculation results reveal that hot electrons could be generated by LSPR at around 715 nm. These hot electrons could reduce the recombination rate of photoinduced carriers and produce more oxygen vacancies for CO_2 reduction. Ma's group studied the mechanisms of photothermal conversion of CO_2 using Fe-based

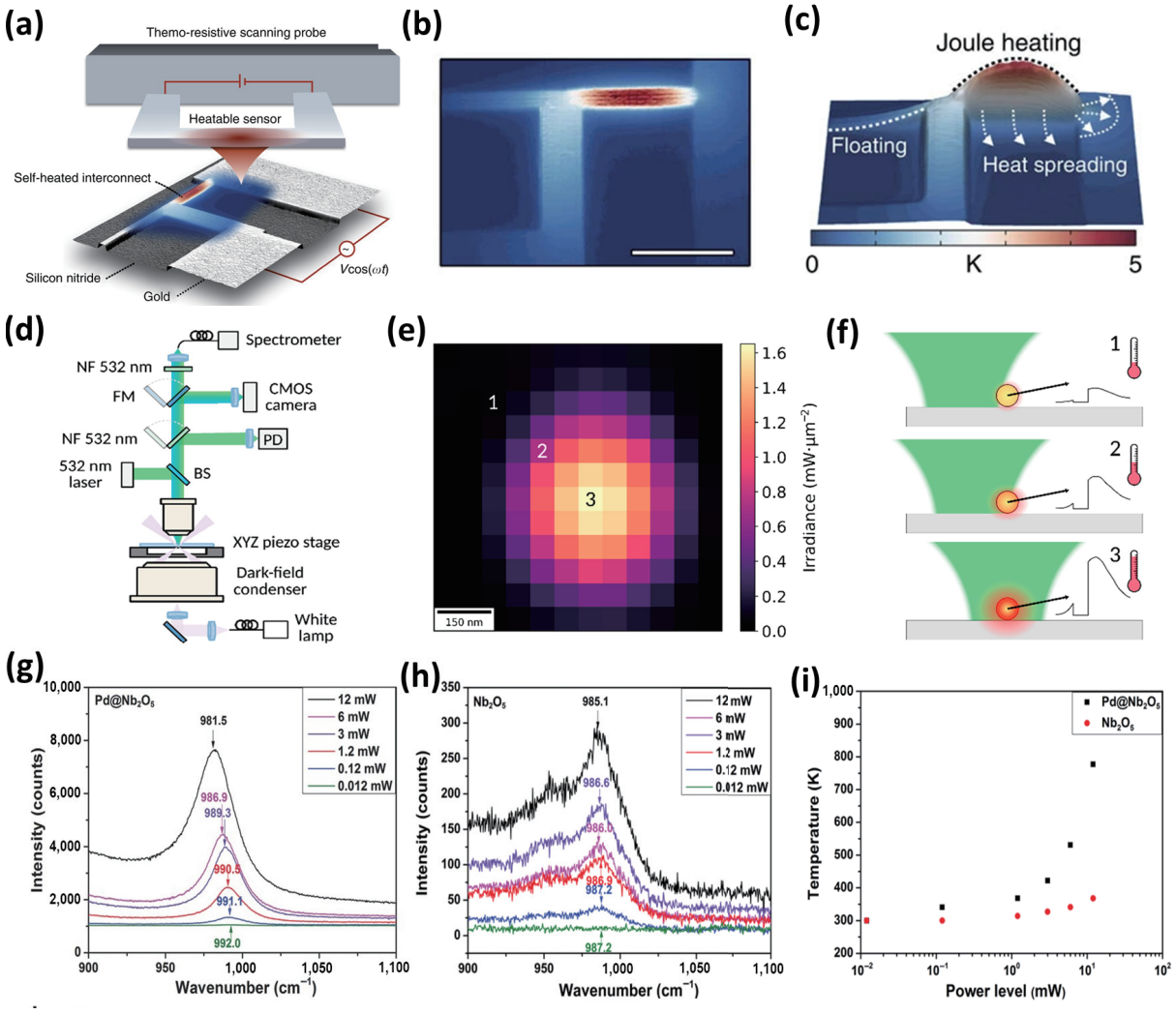

Figure 7 Thermometry characterizations in PTC. (a) Schematic of the thermoresistive scanning probe in contact with a self-heated gold (Au) interconnect (~ 100 nm wide) on a silicon (111) substrate wafer covered with 150 nm of amorphous silicon nitride (SiN_x). An alternating voltage bias ($V\cos(\omega t)$) is applied to modulate the sample temperature. The sample temperature field (red-blue colour scheme indicates the temperature from hot to cold) is inferred by simultaneously probing a time-dependent and a time-averaged heat flux signal between the heatable (red coloured) sensor and the temperature-modulated sample. (b) The true sample temperature rise. This relative temperature increase can be encoded in terms of both height and colour as shown (c). Reproduced with permission from Ref. [94], © Menges, F. et al. 2016. (d) Scheme of the experimental setup to obtain spectra vs. irradiance from a single hyperspectral image. BS: beam splitter. PD: photodiode. NF: notch filter. FM: flipper mirror. (e) Confocal image of an 80 nm Au NP color coded in terms of irradiance on the NP. (f) Schematic illustration of the heating of a NP during scanning, along with example PL spectra from pixels 1 to 3 marked in (e). Reproduced with permission from Ref. [96], © American Chemical Society 2020. Dependence of the Raman frequency for νNb=O stretching vibrations of (g) $Pd@Nb_2O_5$ and (h) Nb_2O_5 nanorods at different power levels. (i) Estimated temperatures for $Pd@Nb_2O_5$ and Nb_2O_5 at different power levels. Reproduced with permission from Ref. [81], © Jia, J. et al. 2016.

catalysts via DFT calculations (Figs. 8(b) and 8(c)) [100]. The calculated adsorption energies confirmed the differences in CO adsorption and H_2 dissociation capabilities over Fe_3C and Fe_2O_4 catalysts. These results are in accordance with the experimental findings and expected reaction pathways are proposed with both thermal and non-thermal effects of light.

It is worth noting that the discussed methodologies can only help to differentiate the photochemical and thermochemical contributions to some extent. Usually, they facilitate the identification of one being the dominant mechanism and the other being the enhancement factor. The complete decoupling of heat and light contributions with multiple effects in PTC catalytic reactions is still challenging. Synergetic contributions to the overall catalytic activity require more investigations and in-depth understanding of the mechanisms.

5 Design considerations of photothermal catalysts

The synergetic photothermal enhancement of both photocatalysis and thermocatalysis has been widely demonstrated. They do not always complement each other to achieve constructive outcomes, such as carrier recombination at high temperature due to no efficient carrier transfer path [101], undesirable desorption of reactants due to thermalization of hot electrons [102], and unfavorable selectivity [103]. Therefore, the rational design of the photothermal catalysts is critical. Both the intrinsic properties of the photothermal material and the structural engineering of the catalyst need to be carefully considered when constructing the photothermal catalyst. In this section, design criteria are first introduced followed by the discussion on various befitting architectural designs of photothermal catalysts.

5.1 Catalyst design criteria

In order to design an effective photothermal catalyst for enhanced activity, a few requirements on top of their conventional catalytic properties need to be fulfilled, namely (1) broadband solar absorption, (2) high photothermal conversion efficiency, (3) heat transfer and confinement at the active sites, (4) uncompromised or unblocked active sites, and (5) desirable photoinduced carrier

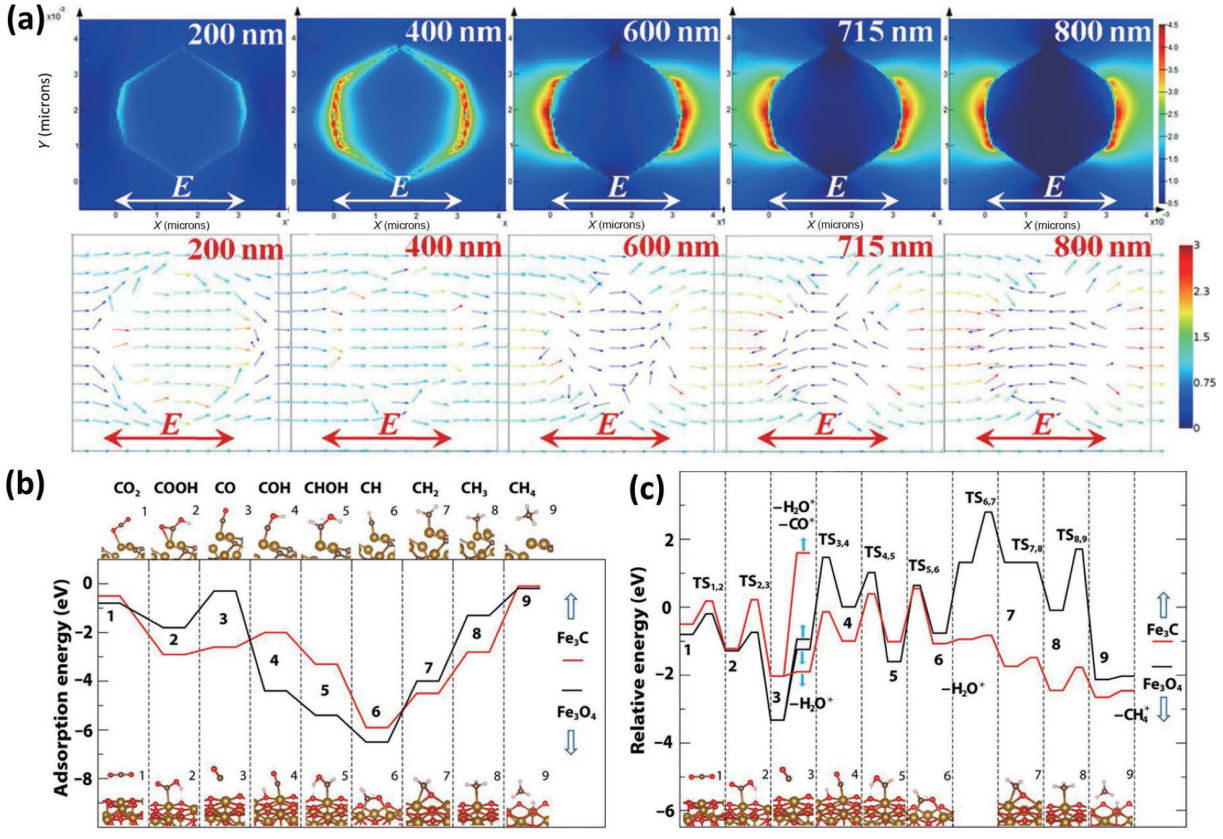

Figure 8 Computational studies in PTC. (a) Spatial distribution of the LSPR-induced enhancement of the electric field intensity from the FDTD simulations for palladium-nanoparticle-loaded TiO_2 at excitation wavelengths and the electric-field vector at excitation wavelengths. Here, *E* denotes the vector of the electric field. Reproduced with permission from Ref. [78], © American Chemical Society 2018. (b) and (c) Reaction paths for CO_2 hydrogenation on Fe_3O_4 and Fe_3C surfaces. (b) Adsorption energy and (c) Gibbs energy of the reaction (red ball: O, gold ball: Fe, little gray ball: C, and little white ball: H). Reproduced with permission from Ref. [100], © American Chemical Society 2020.

generation and transfer path. The first two are the key criteria for photothermal catalysis and mainly depend on the nature and structure of the photothermal materials. Commonly used photothermal materials include plasmonic metals, narrow bandgap semiconductors, carbon-based nanomaterials, etc. [1, 104, 105]. The optical properties can be tuned by shape, size, and composition of the materials to achieve optimized photothermal conversion efficiency and hot carrier generation. The heat generated by the photothermal materials needs to be transferred or retained at the active site for catalytic reaction, instead of losing to the surroundings [106]. The photothermal heating component demands high thermal conductivity for heat dissipation to the active sites, while the catalyst favors low thermal conductivity for heat confinement at the active sites. A typical strategy is to enclose the catalyst with a layer of thermal insulative coating to reduce heat loss [91, 107]. Moreover, the support materials are often employed to enhance the catalytic activity and stability of the catalyst. The heat transport from or to the support based on various architectural catalyst designs is also an important factor to be considered in photothermal catalysis. The active sites on the surface of the catalyst are where the adsorption and activation of the reactant molecules occurs, thus the number of active sites is a critical factor that affects the catalytic activity [33]. The incorporation of the photothermal heating component should avoid blocking the active sites. In the case that the photothermal heating component itself is also an active catalyst, increasing surface area, introducing support materials such as metal oxides, and adding co-catalysts will create more active sites. Furthermore, the photoinduced carriers generated from the photothermal heating component, such as plasmonic metals or semiconductors, could facilitate charge transfer or take part in the catalytic reaction including the adsorption of reactant, the activation of chemical bonds, the conversion of intermediate species, and desorbing harmful surface species. Proper selections of the materials with appropriate band alignment and photoinduced carrier energy will lead to desirable carrier transfer path and enhanced catalytic activity, selectivity and stability. In addition, other characteristics, such as compatibility with the catalyst, long-term stability at elevated temperature, and high surface area, are important factors to consider when designing photothermal catalysts.

5.2 Catalyst architectural design

Based on the aforementioned criteria, an effective photothermal catalytic system should consist of the following components: (1) main catalyst where key active sites are located; (2) photothermal heating material to assist in the surface reaction; and (3) support material for catalyst dispersion and/or increasing the surface area for accessibility. Three photothermal catalyst architectures are proposed in this review (Fig. 9). The first design is utilizing the photothermal heating effect of the active catalyst, meaning the catalyst itself is also a light-absorbing material as such the photothermal heating and catalytic reaction occur on the same material, thus referred as dual-function catalyst. The other two designs are hybrid catalysts, one is adopting support material as the photothermal heating medium, and heat is transferred to the catalyst; the other is introducing separate material as the photothermal heating center, and heat is transferred to the support which in this case provides the active sites for the conversion reaction. In the first design, it is more complicated for discernment and differentiation of various mechanisms as multiple processes happen concurrently on the same material. In comparison, the latter two hybrid designs in which light

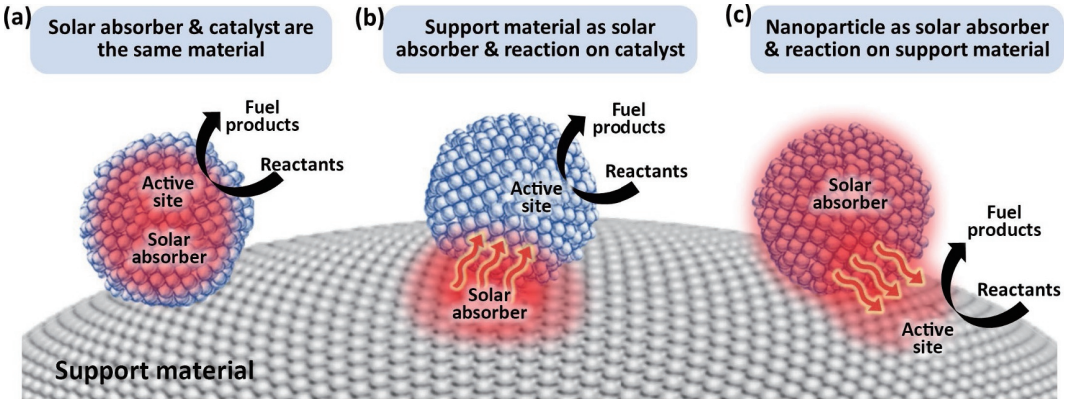

Figure 9 Various types of architectural catalyst design for photothermal catalytic fuel production.

absorption and catalytic reaction are dissociated, provide more controllability for process optimization [20]. The proposed designs offer a general guideline, but each component may not be restricted to a unique function, and other components such as co-catalyst may also exist in the catalytic system [6].

5.2.1 *Dual-function catalyst*

Photothermal catalysts are generally composed of support (e.g., typical supports without light response like SiO_2 and Al_2O_3, and semiconductors with light absorption and activation like TiO_2, $SrTiO_3$, $BaTiO_3$, and In_2O_3) embraced with a metal (e.g., noble metal like Ru, Rh, Au, and Pt, or non-noble metal like Fe, Co, Ni, and Cu) constitution [84, 108]. Generally, these supported metals or metal oxides play dual roles in the photothermal catalysis reaction, including the light absorber and active sites [90, 109]. In order to confine the heat at the active sites, heat dissipation should be minimized in dual-function catalyst. Cai et al. constructed core–shell structured Ni@nanoporous SiO_2 for photothermal methanation and RWGS [91]. Ni metals contributed to the light absorption and resulted in the temperature gradients from the photothermal effects, in conjunction with serving as the active sites for methanation and RWGS reaction (Fig. 10(a)). The coating of a nanoporous silica sheath protected the encapsulated Ni metals against heat dissipation under high temperature. Moreover, the utilization of support materials with high surface areas is favoured to increase the dispersion and stability of metal active sites, contributing to enhanced photothermal activity and durability (Fig. 10(b)). For example, Ren et al. exfoliated ultrathin Mg-Al layered double hydroxide (LDH) nanosheets matrix and loaded with Ru nanoparticles for activating CO_2 and H_2 in thermal and T-PTC [110]. The two-dimensional LDH structure provided abundant sites for adsorption and activation of CO_2 and Ru acted as the local heater and active sites for H_2 cleavage. Other than metal materials, semiconductors have also been demonstrated as dual-function catalysts. Li et al. found that the LSPR effect induced by oxygen vacancies narrowed the bandgap of MoO_3 and extended its absorption range to the infrared region [59]. As a result, MoO_{3-x} obtained enhanced photothermal CO_2 reduction with 20- and 52-times higher than that of MoO_3 in terms of CO and CH_4 production rates respectively.

5.2.2 *Hybrid catalyst*

Hybrid catalyst combines the functions of two or more components to improve the overall photothermal catalytic performance [20]. Researchers have utilized the support materials which are common in gas-phase catalytic reactions for photothermal heating. Different from traditional functions of supports, some rational designs of incorporating black colour materials or light responsive photocatalysts to serve as supports are employed to further increase the photo-response of metal nanoparticles [111]. In hydride catalyst, efficient heat transfer to the active sites is needed. In order to maximize the temperature of the solar absorber, high absorption over the solar spectrum and low emissivity in the mid-infrared region are preferred. Hoch et al. used photoactive SiNWs as supports to coat $In_2O_{3-x}(OH)_y$ nanoparticles to reach a temperature of 150 °C under light illumination (Fig. 10(c)) [41]. Li et al. confined single atom Ni into the ultrathin amorphous Y_2O_3 nanosheets to attain a temperature of 288 °C due to the excellent light absorption and low thermal radiation of selective absorber Y_2O_3 [92]. As a result, the thermochemistry driven photothermal methanation conversion of more than 80% over Ni/Y_2O_3 nanosheets was achieved under ambient sunlight. TiO_2 or titanium perovskite $SrTiO_3$, although can only absorb UV light which accounts for only 5% of the total solar spectrum, works as supports and contributes to the photothermal activity from the perspective of thermochemistry and photochemistry. Mateo et al. designed RuO_2 nanoparticles as the active sites and $SrTiO_3$ support to promote charge separation and thus efficiently improve the methanation process under UV–vis irradiation at 150 °C [112]. Noticeably, different supports work distinctively depending on the metal active sites. Cho and co-authors reported visible light driven DRM over various semiconductors support materials and found Rh-loaded TaON catalyst delivered the highest activity [113]. The bandgap excitation as well as the recombination of electrons and holes over TaON support contributed to the efficient DRM reaction.

Another design of the hybrid catalyst is incorporating light-absorbing nanomaterials as the promoter for the reaction via photothermal effects. Li et al. synthesized $C@TiO_2/TiO_{2-x}$ yolk–shell nanoreactor for a solar water splitting system [114]. The carbon core extends the light absorption to the near-infrared range and functions as a heat generator via its photothermal effect, while the TiO_2/TiO_{2-x} forms a homojunction for enhanced charge transfer to the active sites on TiO_{2-x} surface. The as-prepared catalyst enhances the activity by 22 times compared with pure TiO_{2-x}. Zhang et al. designed Ag-ZrO_2 photocatalyst for CO_2 reduction with H_2 [115]. The LSPR at the Ag surface raises the temperature from 286 to 392 K, which efficiently activated H_2. The H atoms then spill over to the bicarbonate species, and combine with separated electrons and holes above ZrO_2 (Fig. 10(d)). In this hybrid design, when photochemistry is involved in the catalytic reaction, especially in the case when the reaction is driven by photoinduced carriers, light penetration into the catalyst and reaching to the active sites needs to be carefully considered. With the presence of a photothermal heating component that often has strong optical absorption capability and/or broad absorption range, the light reaching the catalyst may be compromised. To optimize the light absorption of the catalyst, the photothermal heating component needs to be fabricated into thin films, or rationally designed with selective solar absorption. Ho's group

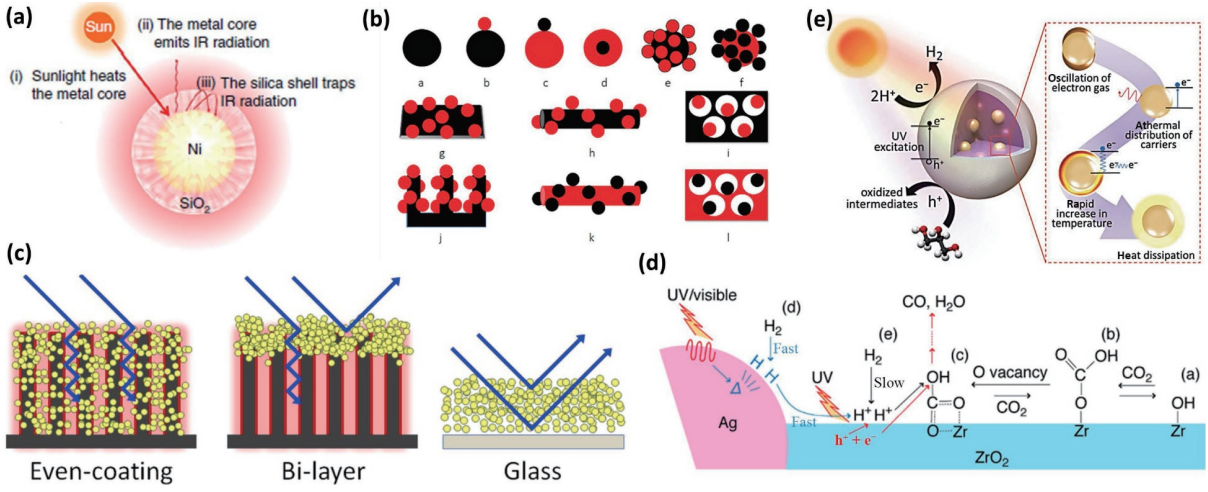

Figure 10 Various catalyst architectural designs in PTC. (a) Schematic of the nanoscale greenhouse effect in Ni@nanoporous SiO_2. Reproduced with permission from Ref. [91], © Cai, M. J. et al. 2021. (b) Illustration of a library of photothermal nanoscale architectures where the black objects refer to a broadband light absorber that can function as nanoheater/catalyst and the red objects as the catalyst. Reproduced with permission from Ref. [6], © The Royal Society of Chemistry 2019. (c) Schematic illustration of the effect of nano architecturing on the film's interaction with incident light. The blue arrows represent incident solar irradiation, and the red shading for the evenly coated and bilayer $In_2O_{3-x}(OH)_y$/SiNW films illustrates photothermal heat generation. Reproduced with permission from Ref. [41], © American Chemical Society 2016. (d) Proposed intermediate species starting from CO_2 and H_2 to CO during CO_2 exchange and photocatalytic CO_2 reduction. Reproduced with permission from Ref. [115], © American Chemical Society 2019. (e) Schematic diagram of the proposed mechanism of SiO_2/Ag@TiO_2 core–shell nanocomposites for photothermal catalytic hydrogen generation. Reproduced with permission from Ref. [42], © The Royal Society of Chemistry 2016.

designed a core–shell structure photothermal catalyst with the core as the solar absorber for localized heating and the photoactive shell for the catalytic reaction (Fig. 10(e)) [42]. With this design, the high-energy photons from the incident light will be absorbed by the TiO_2 shell to generate photoinduced carriers, while the lower energy photons transmitted through the shell are absorbed by the solar absorber core. Heat generated by the core through photothermal conversion provides localized heating for enhanced catalytic hydrogen production. Moreover, additional effects on catalytic activity may be introduced when a catalytic material is blended with a nanostructured solar absorber. For example, extra routes for the charge transfer and additional photoinduced carries may be formed when plasmonic metal nanoparticles are loaded on the catalyst. This may be destructive to the carrier transfer path to active sites, or beneficial for the activation of the adsorbents, selectivity of the desirable products, and stability of the catalyst as discussed earlier. By tuning the energy of the photoinduced carriers to match specific electronic states and/or vibrational modes of adsorbates or intermediates, the specific elementary steps of the chemical reaction can be manipulated for improved performances and alternate catalytic pathways [90].

6 Applications for fuel generation

Solar-driven catalysis based on the concept of utilizing solar energy as the source of light and heat offers an alternative sustainable and green path for energy conversion and/or storage. This photothermal catalysis with rationally designed nanostructured catalysts is a promising strategy for various catalytic fuel production. Solar fuel generation through photothermal catalysis mainly includes hydrogen generation from water splitting and carbon-based fuel from CO_2 reduction process. In this section, photothermal catalytic processes for producing fuels will be discussed.

6.1 H_2 production from water

Hydrogen, as one of the high-density energy carriers for clean energy, is a potential candidate for sustainable development. Photocatalysis is the most direct route for hydrogen production, in which solar energy is used to convert water into hydrogen in the presence of photocatalyst [24]. However, the narrow band solar absorption of the photocatalyst often limits its conversion efficiency. On the other hand, the solar-thermal water splitting often requires an extremely high reaction temperature. Recently, the synergetic effects of photochemistry and thermochemistry greatly enhanced the hydrogen production rate from water under mild reaction conditions.

It has been demonstrated that increased temperature has a positive effect on photocatalytic hydrogen generation. Song et al. reported the hydrogen generation rate of Ni_2P/TiO_2 with methanol aqueous solution increases by ~ 3.6 times when the temperature increases from 35 to 90 °C (Fig. 11(a)) [116]. The augmented transfer of electrons from TiO_2 to Ni_2P at higher temperature is vital for the enhancement. In Ho's work, various sacrificial reagent has been tested for hydrogen production rate of TiO_2 spheres with increasing temperature [42]. The results reveal that glycerol obtained the highest enhancement (56.6%) followed by ethylene glycol (50.3%), methanol (40.5%), and glucose (13.9%) when temperature increased from 30 to 90 °C (Fig. 11(b)). By using nanostructured Ag@SiO_2 as the solar absorber to convert sunlight into heat confined at the active sites, they achieved a photothermal enhancement of ~ 95% for photocatalytic hydrogen generation without external physical heating. In their following work [62], the spectrally selective designed photochemical and photothermal heating functions of Au-loaded Ag@SiO_2@TiO_2 nanosheets (AST NS-Au) catalyst are demonstrated. The hydrogen generation rate of 30.2 mmol·g^{-1}·h^{-1} which is 74 times higher than the control sample SiO_2@TiO_2 nanosheets (ST NS) is achieved (Fig. 11(c)). This enhanced catalytic activity is attributed to the nonoverlapped light absorption and undisrupted charge transfer rationales of the composite catalyst.

Introducing light can enhance thermal activity and effectively reduce the temperature required for solar-thermal water splitting. Caudillo-Flores et al. examined the activity of Ru/TiO_2 for the gas phase photothermal catalytic hydrogen production [117]. The results clearly demonstrated the synergistic utilization of light and heat. The photothermal activities are consistently higher than the entirety of thermal and photo activities in the temperature range between 120 and 300 °C with the maximum enhancement (~ 50%) achieved at 240 °C. Fang et al. obtained similar results

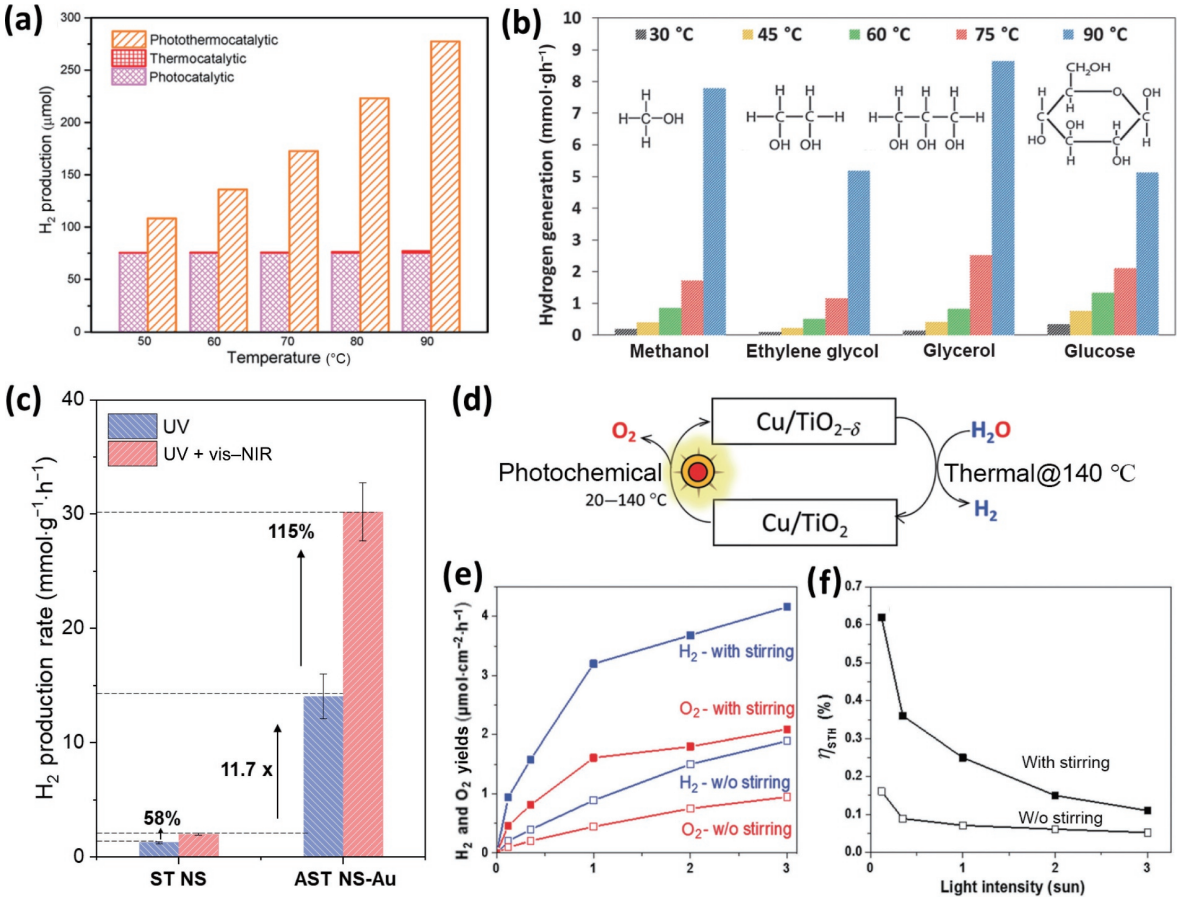

Figure 11 Application of PTC in H_2 production from water. (a) Comparison of 3 h H_2 generation over Ni_2P/TiO_2 under photocatalytic (35 °C), thermocatalytic, and photothermocatalytic (50–90 °C) reaction conditions. System contains 14 mg of Ni_2P/TiO_2 photocatalyst in a 140 mL of aqueous solution containing 20 vol.% methanol. Reproduced with permission from Ref. [116], © American Chemical Society 2018. (b) Hydrogen generation by TiO_2 spheres in methanol (10% v/v), ethylene glycol (25% v/v), glycerol (20% v/v), and glucose (0.5 g) solution at different temperatures. Reproduced with permission from Ref. [42], © The Royal Society of Chemistry 2016. (c) Hydrogen production rates of ST NS and AST NS-Au under UV and full spectrum irradiation. Reproduced with permission from Ref. [62], © Wiley-VCH GmbH 2021. (d) A schematic illustration of the solar photochemical-thermal water splitting with Cu/TiO_2. Plots of (e) the production rates of H_2 (blue) and O_2 (red) and (f) the solar-to-H_2 conversion efficiency with respect to the light intensity under the conditions of stirring and no stirring. Reproduced with permission from Ref. [79], © The Royal Society of Chemistry 2017.

using NiO_x-TiO_2 catalyst for photothermal water splitting with methanol [118]. The maximum enhancement of hydrogen production rate with illumination is obtained at 260 °C, which is 2.5 times more than that without illumination. Docao et al. found that Cu/TiO_2 can expel O_2 at room temperature under 1 Sun irradiation, and the reduced form $Cu/TiO_{2-\delta}$ effectively abstracts O atoms from steam at 140 °C which is much lower than what is needed in conventional solar-thermal water splitting systems (ca. 1,000 °C) (Figs. 11(d)–11(f)) [79]. The two-step H_2O splitting process to generate O_2 and H_2 can be carried out isothermally at 140 °C.

6.2 CO_2 conversion

Photothermal conversion of CO_2 is one of the most straightforward and effective alternative approaches to transform CO_2 into high value-added fuels at mild conditions. H_2O, H_2, and CH_4 are three primary reductants used in the CO_2 conversion, which are corresponding to artificial photosynthesis, hydrogenation, and dry reforming, respectively. Herein, the different applications based on these three types of reactions via photothermal catalysis will be reviewed.

6.2.1 CO_2 reduction with H_2O

CO_2 reduction by water via solar energy to produce solar fuels, such as CO, CH_4, and methanol, simulates the photosynthesis process in nature and thus is known as artificial photosynthesis. However, the current yield based on semiconductor for pure photocatalytic CO_2 reduction is still very low for practical applications. Some photothermal catalytic systems have been reported to further boost the artificial photosynthesis process. Minh et al. synthesized three-dimensional ordered macroporous perovskites $LaSrCoFeO_{6-\delta}$ for CO_2 reduction with H_2O under thermal and S-PTC. Due to the active oxygen vacancies of $LaSrCoFeO_{6-\delta}$ catalysts, it achieved highly efficient CO_2 conversion into CH_4 in the photo-thermo catalytic process, which was 5 times higher than the pure thermocatalytic process [119]. Zhao et al. also reported oxygen deficient WO_3 catalysts for higher CH_4 yield in the S-PTC process when H_2O was used as the reductant (Fig. 12(a)) [120]. These studies indicated the great potentials of photothermal effects on the photosynthesis catalytic process.

6.2.2 CO_2 reduction with H_2

When CO_2 is reduced by H_2, it will produce different products depending on the operating conditions. Here, we will succinctly summarize three applications of CO_2 reduction by H_2 including CO_2 methanation, RWGS, and methanol synthesis, with the corresponding main product of CH_4, CO, and CH_3OH, respectively. CO_2 methanation, also known as the Sabatier reaction, generally requires eight electrons to produce CH_4, and thus poses a high kinetic barrier. Lin and co-workers deposited Ru onto $TiO_{(2-x)}N_x$ support and investigated the thermochemistry

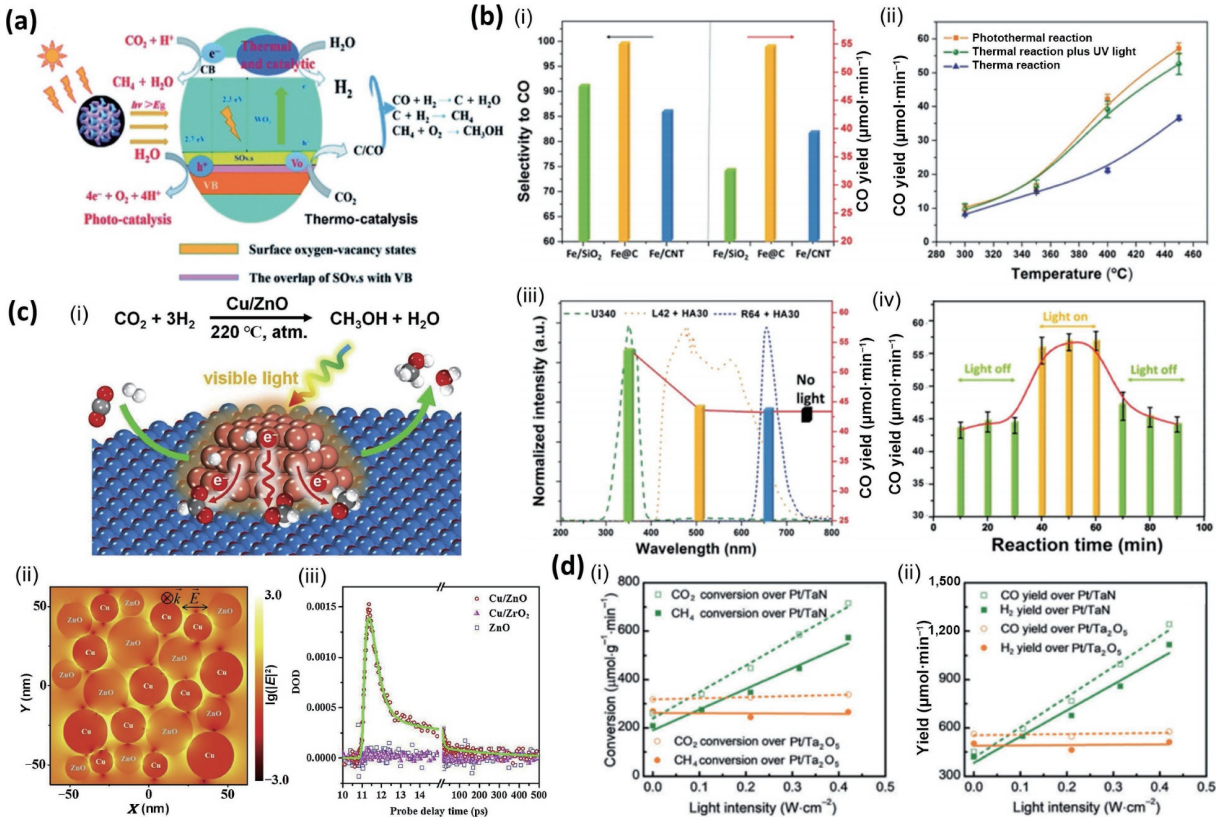

Figure 12 Application of PTC in CO_2 conversion. (a) Schematic diagram of the separate photocatalytic, thermocatalytic and photothermal coupling catalytic reduction of CO_2 over a hydrogen-treated m-WO_3 catalyst in the presence of H_2O. Reproduced with permission from Ref. [120], © The Royal Society of Chemistry 2016. (b) (i) Photoinduced thermo-catalytic CO_2 conversion performance for Fe@C, Fe/SiO_2, and Fe/CNT catalysts in fixed bed reactor. (ii) Contrasts of CO evolution rates for the photoinduced thermal and traditional thermal reactions over Fe@C catalyst. (iii) CO evolution rates over Fe@C without or with light irradiation of different wavelength ranges at 450 °C. (iv) CO evolution rates at 450 °C with and without UV-light illumination over Fe@C catalyst. Reproduced with permission from Ref. [122], © WILEY-VCH Verlag GmbH & Co. KgaA, Weinheim 2016. (c) (i) Methanol synthesis via CO_2 reduction under ambient pressure over plasmonic Cu/ZnO catalysts. (ii) Spatial distribution of the electromagnetic fields over the Cu/ZnO catalyst under 580 nm irradiation stimulated using the FDTD method. (iii) Transient absorption kinetics studies over the Cu/ZnO catalyst under photo-excitation at 580 nm. Reproduced with permission from Ref. [123], © Elsevier B.V. 2019. (d) Catalytic performance of Pt/TaN and Pt/Ta_2O_5 in dry reforming of methane: (i) CO_2 and CH_4 conversions and (ii) CO and H_2 yields. Reproduced with permission from Ref. [127], © WILEY-VCH Verlag GmbH & Co. KgaA, Weinheim 2018.

driven photothermal methanation activity. The oxygen vacancies of $TiO_{(2-x)}N_x$ boost the adsorption and activation of CO_2 reactant while the photoinduced electrons from $TiO_{(2-x)}N_x$ would accumulate onto the surface of Ru, thus accredited to the photo-assisted methanation process [121]. In addition, CO_2 hydrogenation will produce CO when operating at a high temperature, which is the RWGS reaction. CO gas from RWGS together with H_2 from renewable energy can be subsequently transformed into valuable fuels. Zhang et al. realized the light-driven RWGS into CO over Fe@C catalyst deriving from MOF. This strategy coupled light-absorbing materials and catalytic active sites in one material matrix and exemplified higher activity and selectivity towards CO (Fig. 12(b)) [122]. Liquid fuel methanol can be directly synthesized by the CO_2 hydrogenation process at 200–300 °C and 3.5–10 MPa. Some scholars discovered that Cu/ZnO catalyst could be used for thermocatalytic CO_2 conversion to methanol at ambient pressure and further improved when solar energy was introduced. The hot carriers by LSPR on Cu nanoparticles would transfer to ZnO support, and subsequently lower the activation barrier and promote the methanol synthesis activity (Fig. 12(c)) [123]. This result was consistent with Wang's study that the selectivity of methanol using rod-shaped $In_2O_{3-x}(OH)_y$ nanocrystal superstructure as the catalyst almost did not drop when light was on [105, 124]. The CO_2 hydrogenation to CH_4, CO, and CH_3OH is competitive relative to each other, and it is of significance to design a highly efficient catalyst aiming for respective reactions.

6.2.3 *CO_2 reduction with CH_4*

Dry reforming of CO_2 and methane is one effective method to convert two major greenhouse gases to simultaneously produce syngas gas which can be further processed into high value-added chemicals. However, pure thermocatalytic DRM always faces serious metal sintering and carbon formation problems due to the side reactions under high temperature. When photochemistry effects are introduced, the solar energy and photoinduced hot carriers would promote the activation of carbon species, and facilitate the desorption of unwanted intermediates and products, thus improve the activity, selectivity, and stability of the catalyst [125, 126]. Ye's group firstly introduced plasmonic Au as a promoter to enhance the thermochemistry driven photothermal DRM performance based on noble metal Rh supported on SBA-15. Subsequently, PdAu, PdCu, or Pt-based noble metal was designed to take advantage of their alloy structure as well as plasmonic properties for DRM. Pt nanoparticles with commercial TaN as support had significant enhancement in the photo-assisted thermal driven DRM reactions. Due to the optical property and polarity of TaN support, it facilitated the separation of electrons and holes and ultimately contributed to activity enhancement (Fig. 12(d)) [127]. Recently, the photothermal dry reforming reaction based on non-noble metal Ni was widely studied, whereby the Ni particles would play dual roles as active sites as well as light absorbers [128]. Liu and co-workers realized the unique catalysis design of Ni@SiO_2 with different morphologies, including yolk–shell Ni@SiO_2, core–shell Ni@SiO_2, and randomly dispersed

Ni nanocatalyst on SiO_2. All the catalysts showed enhanced DRM activity in the presence of light. Moreover, improved stability could be observed for the core–shell, yolk–shell Ni@SiO_2 catalyst because of the inhibition of carbon formation under light irradiation [129].

7 Conclusions and perspective

With the worsening energy crisis and greenhouse effects, the exploitation and utilization of renewable solar energy is considered as a promising alternative resource. The photothermal catalysis, coupled with solar and heat energy, may overcome the present controversies faced by catalysis. These constitute the efficiency bottleneck, namely limited production rates of pure photocatalysis and the immense energy intake of thermocatalysis. Therefore, this review firstly introduces various mechanisms involving photothermal chemistry in catalytic fuel generation and focuses on the effects of light and heat energy in PTC. Then, we summarized the rational design of materials based on the requirement of light and heat elements. Subsequently, we introduced current characterization techniques aiming to reveal the photochemistry and thermochemistry contribution to the photothermal reactions. Finally, we listed the main applications of photothermal solar fuel production including H_2 generation from water, and CO_2 reduced by H_2O, H_2, and CO. There are still challenges remaining in the future development of solar fuel production through PTC. The conclusions drawn from this review and future perspectives of PTC are identified as follows:

(1) The fundamental mechanisms of the three types of PTC reactions can be classified according to the driving force, namely photocatalytic-driven, thermocatalytic-driven, or the combination of them for fuel generation. The integration of photochemistry and thermochemistry is able to enhance the solar energy utilization of ultraviolet, visible to near infrared of the solar spectrum. Unequivocally, the augmented solar utilization boosts the catalytic activity through improved global/localized heating, mass transfer, reaction kinetics, selectivity, and stability of catalysts. However, there is still a large gap in the development and understanding of the mechanisms regarding the synergistic coupling between photo and thermal contributions in catalysis. The identification of the dominant contribution of light and heat, and the reaction mechanisms of photochemistry and thermochemistry need to be thoroughly investigated.

(2) Photothermal catalysts are generally designed based on light absorption properties from photochemistry and the number of active sites from thermochemistry. The established catalysts system includes a dual-functional catalyst that functions with concurrent heating and catalytic reaction on the same medium, and a hybrid catalyst that proceeds heating and catalytic reaction on different media platforms. To ensure optimal balance between photochemistry and thermochemistry reactivity, the light absorption ability, the photothermal conversion capacity, and heat insulation need to be considered. Current research still largely uses light with high intensity for PTC which limits its practical applications for direct solar-to-fuel generation without solar concentrators. Besides applying high light intensity beyond 1-sun, the catalyst development is trending towards enhanced light absorption, high photothermal conversion efficiency, and low thermal conductivity for efficient utilization of photothermal energy. Moreover, designing unique structures in terms of morphology, defects engineering, and plasmonic promotor to facilitate photoinduced carriers separation, favorable chemical bond formation, and surface reaction kinetics will further enhance the activity of the PTC with tunable selectivity and possibilities of uncovering new pathways for PTC.

(3) In PTC, the catalyst will be characterized based on two aspects, thermochemistry and photochemistry. The respective contributions of the two aspects in PTC can be distinguished to a certain extent with experimental designs under various conditions, thermometry characterizations, and computational simulations. The evaluation of temperature is very important for understanding the mechanism of the reaction. The current available *in-situ* temperature techniques using thermocouple or IR camera may not reflect the actual local temperature on the catalyst surface. Therefore, it is still a challenge to precisely determine the temperature of the catalysts at a nanoscale level to study the thermodynamics and kinetics of photothermal catalysis reactions. Other *in-situ* and atomically confined characterization technologies need to be further developed and explored to study the reaction process of PTC reactions.

(4) PTC has been applied for H_2 production from water splitting, as well as CO_2 reduction by H_2O, H_2, and CO to produce solar fuels. Although substantial works have been reported in the past decade, they are often limited to using lab irradiation sources with high flux light intensity (20–50 times greater than solar energy). Moreover, reactor designs concerning high light utilization efficiency and large irradiation surface area are needed for scale-up applications [130, 131]. In addition, the use of optical lens to concentrate solar energy occupies a large footprint and excessively enlarges the size of the reactor. Together with the natural day/night cycles and temperature variations, these factors make current PTC not practical for industrial applications. Hence, there is still a long way to develop sustainable and commercially viable PTC which includes condensed systems/reactors, inexpensive solar concentrators, and efficient and eco-friendly catalytic materials under feasible operation conditions.

Acknowledgements

The authors gratefully thank the financial support from the A*STAR under its 2019 AME IRG & YIRG Grant Calls, A2083c0059 and Central Gap Fund NRF2020NRF-CG001-023 and TAP25002021-01-01–RIE2025.

References

[1] Wang, Z. J.; Song, H.; Liu, H. M.; Ye, J. H. Coupling of solar energy and thermal energy for carbon dioxide reduction: Status and prospects. *Angew. Chem., Int. Ed.* **2020**, *59*, 8016–8035.

[2] Xu, C. Y.; Hong, J. N.; Sui, P. F.; Zhu, M. N.; Zhang, Y. W.; Luo, J. L. Standalone solar carbon-based fuel production based on semiconductors. *Cell Rep. Phys. Sci.* **2020**, *1*, 100101.

[3] Baffou, G.; Cichos, F.; Quidant, R. Applications and challenges of thermoplasmonics. *Nat. Mater.* **2020**, *19*, 946–958.

[4] Zhang, W. J.; Ma, D.; Pérez-Ramírez, J.; Chen, Z. P. Recent progress in materials exploration for thermocatalytic, photocatalytic, and integrated photothermocatalytic CO_2-to-fuel conversion. *Adv. Energy Sustainability Res.* **2022**, *3*, 2100169.

[5] Hong, J. N.; Xu, C. Y.; Deng, B. W.; Gao, Y.; Zhu, X.; Zhang, X. H.; Zhang, Y. W. Photothermal chemistry based on solar energy: From synergistic effects to practical applications. *Adv. Sci.* **2022**, *9*, 2103926.

[6] Ghoussoub, M.; Xia, M. K.; Duchesne, P. N.; Segal, D.; Ozin, G. Principles of photothermal gas-phase heterogeneous CO_2 catalysis. *Energy Environ. Sci.* **2019**, *12*, 1122–1142.

[7] Zhu, L. L.; Gao, M. M.; Peh, C. K. N.; Ho, G. W. Solar-driven photothermal nanostructured materials designs and prerequisites for evaporation and catalysis applications. *Mater. Horiz.* **2018**, *5*, 323–343.

[8] Yang, Y.; Zhao, S. H.; Cui, L. F.; Bi, F. K.; Zhang, Y. N.; Liu, N.; Wang, Y. X.; Liu, F. D.; He, C.; Zhang, X. D. Recent advancement and future challenges of photothermal catalysis for VOCs elimination: From catalyst design to applications. *Green Energy Environ.*, in press, https://doi.org/10.1016/j.gee.2022.02.006.

[9] Zheng, Y. K.; Zhang, L.; Guan, J.; Qian, S. Y.; Zhang, Z. X.; Ngaw, C. K.; Wan, S. L.; Wang, S.; Lin, J. D.; Wang, Y. Controlled synthesis of Cu^0/Cu_2O for efficient photothermal catalytic conversion of CO_2 and H_2O. *ACS Sustainable Chem. Eng.* **2021**, *9*, 1754–1761.

[10] Nair, V.; Muñoz-Batista, M. J.; Fernández-García, M.; Luque, R.; Colmenares, J. C. Thermo-photocatalysis: Environmental and energy applications. *ChemSusChem* **2019**, *12*, 2098–2116.

[11] Li, X. J.; Zhao, S. Y.; Duan, X. G.; Zhang, H. Y.; Yang, S. Z.; Zhang, P. P.; Jiang, S. P.; Liu, S. M.; Sun, H. Q.; Wang, S. B. Coupling hydrothermal and photothermal single-atom catalysis toward excellent water splitting to hydrogen. *Appl. Catal. B:Environ.* **2021**, *283*, 119660.

[12] Mateo, D.; Morlanes, N.; Maity, P.; Shterk, G.; Mohammed, O. F.; Gascon, J. Efficient visible-light driven photothermal conversion of CO_2 to methane by nickel nanoparticles supported on barium titanate. *Adv. Funct. Mater.* **2020**, *31*, 2008244.

[13] Mateo, D.; Cerrillo, J. L.; Durini, S.; Gascon, J. Fundamentals and applications of photo-thermal catalysis. *Chem. Soc. Rev.* **2021**, *50*, 2173–2210.

[14] Li, H. K.; Dang, C. X.; Yang, G. X.; Cao, Y. H.; Wang, H. J.; Peng, F.; Yu, H. Bi-functional particles for integrated thermo-chemical processes: Catalysis and beyond. *Particuology* **2021**, *56*, 10–32.

[15] Yang, Y. Y.; Feng, H. P.; Niu, C. G.; Huang, D. W.; Guo, H.; Liang, C.; Liu, H. Y.; Chen, S.; Tang, N.; Li, L. Constructing a plasma-based Schottky heterojunction for near-infrared-driven photothermal synergistic water disinfection: Synergetic effects and antibacterial mechanisms. *Chem. Eng. J.* **2021**, *426*, 131902.

[16] Li, N. X.; Tu, Y.; Wang, K.; Huang, D. X.; Shen, Q. H.; Chen, W. S.; Zhou, J. C.; Ma, Q. H.; Liu, M. C. Construction of a photo-thermal-magnetic coupling reaction system for enhanced CO_2 reduction to CH_4. *Chem. Eng. J.* **2021**, *421*, 129940.

[17] Wang, S. H.; Tountas, A. A.; Pan, W. B.; Zhao, J. J.; He, L.; Sun, W.; Yang, D. R.; Ozin, G. A. CO_2 footprint of thermal versus photothermal CO_2 catalysis. *Small* **2021**, *17*, 2007025.

[18] Zhang, F.; Li, Y. H.; Qi, M. Y.; Yamada, Y. M. A.; Anpo, M.; Tang, Z. R.; Xu, Y. J. Photothermal catalytic CO_2 reduction over nanomaterials. *Chem Catal.* **2021**, *1*, 272–297.

[19] Kho, E. T.; Tan, T. H.; Lovell, E.; Wong, R. J.; Scott, J.; Amal, R. A review on photo-thermal catalytic conversion of carbon dioxide. *Green Energy Environ.* **2017**, *2*, 204–217.

[20] Xie, B. Q.; Lovell, E.; Tan, T. H.; Jantarang, S.; Yu, M. Y.; Scott, J.; Amal, R. Emerging material engineering strategies for amplifying photothermal heterogeneous CO_2 catalysis. *J. Energy Chem.* **2021**, *59*, 108–125.

[21] Luo, S. Q.; Ren, X. H.; Lin, H. W.; Song, H.; Ye, J. H. Plasmonic photothermal catalysis for solar-to-fuel conversion: Current status and prospects. *Chem. Sci.* **2021**, *12*, 5701–5719.

[22] Xiao, J. D.; Jiang, H. L. Metal-organic frameworks for photocatalysis and photothermal catalysis. *Acc. Chem. Res.* **2019**, *52*, 356–366.

[23] Gao, M. M.; Zhu, L. L.; Peh, C. K.; Ho, G. W. Solar absorber material and system designs for photothermal water vaporization towards clean water and energy production. *Energy Environ. Sci.* **2019**, *12*, 841–864.

[24] Ma, R.; Sun, J.; Li, D. H.; Wei, J. J. Review of synergistic photo-thermo-catalysis: Mechanisms, materials and applications. *Int. J. Hydrog. Energy* **2020**, *45*, 30288–30324.

[25] Wang, F. F.; Huang, Y. J.; Chai, Z. G.; Zeng, M.; Li, Q.; Wang, Y.; Xu, D. S. Photothermal-enhanced catalysis in core–shell plasmonic hierarchical Cu_7S_4 microsphere@zeolitic imidazole framework-8. *Chem. Sci.* **2016**, *7*, 6887–6893.

[26] Kim, C.; Hyeon, S.; Lee, J.; Kim, W. D.; Lee, D. C.; Kim, J.; Lee, H. Energy-efficient CO_2 hydrogenation with fast response using photoexcitation of CO_2 adsorbed on metal catalysts. *Nat. Commun.* **2018**, *9*, 3027.

[27] Wang, Q.; Domen, K. Particulate photocatalysts for light-driven water splitting: Mechanisms, challenges, and design strategies. *Chem. Rev.* **2020**, *120*, 919–985.

[28] Du, S. H.; Bian, X. N.; Zhao, Y. X.; Shi, R.; Zhang, T. R. Progress and prospect of photothermal catalysis. *Chem. Res. Chin. Univ.* **2022**, *38*, 723–734.

[29] Zhang, Y. W.; Xu, C. Y.; Chen, J. C.; Zhang, X. H.; Wang, Z. H.; Zhou, J. H.; Cen, K. F. A novel photo-thermochemical cycle for the dissociation of CO_2 using solar energy. *Appl. Energy* **2015**, *156*, 223–229.

[30] Xie, T.; Zhang, Z. Y.; Zheng, H. Y.; Xu, K. D.; Hu, Z.; Lei, Y. Enhanced photothermal catalytic performance of dry reforming of methane over Ni/mesoporous TiO_2 composite catalyst. *Chem. Eng. J.* **2022**, *429*, 132507.

[31] Chen, G. B.; Waterhouse, G. I. N.; Shi, R.; Zhao, J. Q.; Li, Z. H.; Wu, L. Z.; Tung, C. H.; Zhang, T. R. From solar energy to fuels: Recent advances in light-driven C_1 chemistry. *Angew. Chem., Int. Ed.* **2019**, *58*, 17528–17551.

[32] Xu, Y. F.; Duchesne, P. N.; Wang, L.; Tavasoli, A.; Jelle, A. A.; Xia, M. K.; Liao, J. F.; Kuang, D. B.; Ozin, G. A. High-performance light-driven heterogeneous CO_2 catalysis with near-unity selectivity on metal phosphides. *Nat. Commun.* **2020**, *11*, 5149.

[33] Song, C. Q.; Wang, Z. H.; Yin, Z.; Xiao, D. Q.; Ma, D. Principles and applications of photothermal catalysis. *Chem Catal.* **2022**, *2*, 52–83.

[34] Li, Z.; Zhang, X. H.; Zhang, L.; Xu, C. Y.; Zhang, Y. W. Pathway alteration of water splitting via oxygen vacancy formation on anatase titanium dioxide in photothermal catalysis. *J. Phys. Chem. C* **2020**, *124*, 26214–26221.

[35] Zhang, M. T.; Wang, M.; Xu, B. J.; Ma, D. How to measure the reaction performance of heterogeneous catalytic reactions reliably. *Joule* **2019**, *3*, 2876–2883.

[36] Shoji, S.; Peng, X. B.; Yamaguchi, A.; Watanabe, R.; Fukuhara, C.; Cho, Y.; Yamamoto, T.; Matsumura, S.; Yu, M. W.; Ishii, S. et al. Photocatalytic uphill conversion of natural gas beyond the limitation of thermal reaction systems. *Nat. Catal.* **2020**, *3*, 148–153.

[37] Linic, S.; Aslam, U.; Boerigter, C.; Morabito, M. Photochemical transformations on plasmonic metal nanoparticles. *Nat. Mater.* **2015**, *14*, 567–576.

[38] Li, Z.; Zhang, L.; Huang, W. H.; Xu, C. Y.; Zhang, Y. W. Photothermal catalysis for selective CO_2 reduction on the modified anatase TiO_2 (101) surface. *ACS Appl. Energy Mater.* **2021**, *4*, 7702–7709.

[39] Zhu, Z. Z.; Guo, W. Y.; Zhang, Y.; Pan, C. S.; Xu, J.; Zhu, Y. F.; Lou, Y. Research progress on methane conversion coupling photocatalysis and thermocatalysis. *Carbon Energy* **2021**, *3*, 519–540.

[40] Wang, F.; Li, C. H.; Chen, H. J.; Jiang, R. B.; Sun, L. D.; Li, Q.; Wang, J. F.; Yu, J. C.; Yan, C. H. Plasmonic harvesting of light energy for Suzuki coupling reactions. *J. Am. Chem. Soc.* **2013**, *135*, 5588–5601.

[41] Hoch, L. B.; O'Brien, P. G.; Jelle, A.; Sandhel, A.; Perovic, D. D.; Mims, C. A.; Ozin, G. A. Nanostructured indium oxide coated silicon nanowire arrays: A hybrid photothermal/photochemical approach to solar fuels. *ACS Nano* **2016**, *10*, 9017–9025.

[42] Gao, M. M.; Connor, P. K. N.; Ho, G. W. Plasmonic photothermic directed broadband sunlight harnessing for seawater catalysis and desalination. *Energy Environ. Sci.* **2016**, *9*, 3151–3160.

[43] Han, B.; Wei, W.; Chang, L.; Cheng, P. F.; Hu, Y. H. Efficient visible light photocatalytic CO_2 reforming of CH_4. *ACS Catal.* **2016**, *6*, 494–497.

[44] Yuan, D. C.; Peng, Y. H.; Ma, L. P.; Li, J. C.; Zhao, J. G.; Hao, J. J.; Wang, S. F.; Liang, B. L.; Ye, J. H.; Li, Y. G. Coke and sintering resistant nickel atomically doped with ceria nanosheets for highly efficient solar driven hydrogen production from bioethanol. *Green Chem.*, **2022**, *24*, 2044–2050.

[45] Li, Y. G.; Bai, X. H.; Yuan, D. C.; Zhang, F. Y.; Li, B.; San, X. Y.; Liang, B. L.; Wang, S. F.; Luo, J.; Fu, G. S. General heterostructure strategy of photothermal materials for scalable solar-heating hydrogen production without the consumption of artificial energy. *Nat. Commun.* **2022**, *13*, 776.

[46] Meng, X. G.; Wang, T.; Liu, L. Q.; Ouyang, S. X.; Li, P.; Hu, H.

L.; Kako, T.; Iwai, H.; Tanaka, A.; Ye, J. H. Photothermal conversion of CO_2 into CH_4 with H_2 over Group VIII nanocatalysts: An alternative approach for solar fuel production. *Angew. Chem., Int. Ed.* **2014**, *53*, 11478–11482.

[47] Rej, S.; Mascaretti, L.; Santiago, E. Y.; Tomanec, O.; Kment, Š.; Wang, Z. M.; Zbořil, R.; Fornasiero, P.; Govorov, A. O.; Naldoni, A. Determining plasmonic hot electrons and photothermal effects during H_2 evolution with TiN-Pt nanohybrids. *ACS Catal.* **2020**, *10*, 5261–5271.

[48] Takami, D.; Ito, Y.; Kawaharasaki, S.; Yamamoto, A.; Yoshida, H. Low temperature dry reforming of methane over plasmonic Ni photocatalysts under visible light irradiation. *Sustainable Energy Fuels* **2019**, *3*, 2968–2971.

[49] Nguyen, N. T.; Yan, T. J.; Wang, L.; Loh, J. Y. Y.; Duchesne, P. N.; Mao, C. L.; Li, P. C.; Jelle, A. A.; Xia, M. K.; Ghoussoub, M. et al. Plasmonic titanium nitride facilitates indium oxide CO_2 photocatalysis. *Small* **2020**, *16*, 2005754.

[50] Aslam, U.; Rao, V. G.; Chavez, S.; Linic, S. Catalytic conversion of solar to chemical energy on plasmonic metal nanostructures. *Nat. Catal.* **2018**, *1*, 656–665.

[51] Chen, X.; Li, Q.; Zhang, M.; Li, J. J.; Cai, S. C.; Chen, J.; Jia, H. P. MOF-templated preparation of highly dispersed Co/Al_2O_3 composite as the photothermal catalyst with high solar-to-fuel efficiency for CO_2 methanation. *ACS Appl. Mater. Interfaces* **2020**, *12*, 39304–39317.

[52] Peh, C. K. N.; Gao, M. M.; Ho, G. W. Harvesting broadband absorption of the solar spectrum for enhanced photocatalytic H_2 generation. *J. Mater. Chem. A* **2015**, *3*, 19360–19367.

[53] Hoch, L. B.; Wood, T. E.; O'Brien, P. G.; Liao, K.; Reyes, L. M.; Mims, C. A.; Ozin, G. A. The rational design of a single-component photocatalyst for gas-phase CO_2 reduction using both UV and visible light. *Adv. Sci.* **2014**, *1*, 1400013.

[54] Li, Y. Y.; Peng, Y. K.; Hu, L. S.; Zheng, J. W.; Prabhakaran, D.; Wu, S.; Puchtler, T. J.; Li, M.; Wong, K. Y.; Taylor, R. A. et al. Photocatalytic water splitting by N-TiO_2 on MgO (111) with exceptional quantum efficiencies at elevated temperatures. *Nat. Commun.* **2019**, *10*, 4421.

[55] Li, Y. Y.; Wang, C. H.; Song, M.; Li, D. S.; Zhang, X. T.; Liu, Y. C. TiO_{2-x}/CoO_x photocatalyst sparkles in photothermocatalytic reduction of CO_2 with H_2O steam. *Appl. Catal. B:Environ.* **2019**, *243*, 760–770.

[56] Chen, G. B.; Gao, R.; Zhao, Y. F.; Li, Z. H.; Waterhouse, G. I. N.; Shi, R.; Zhao, J. Q.; Zhang, M. T.; Shang, L.; Sheng, G. Y. et al. Alumina-supported CoFe alloy catalysts derived from layered-double-hydroxide nanosheets for efficient photothermal CO_2 hydrogenation to hydrocarbons. *Adv. Mater.* **2018**, *30*, 1704663.

[57] Pan, F. P.; Xiang, X. M.; Deng, W.; Zhao, H. L.; Feng, X. H.; Li, Y. A novel photo-thermochemical approach for enhanced carbon dioxide reforming of methane. *ChemCatChem* **2018**, *10*, 940–945.

[58] Linic, S.; Christopher, P.; Ingram, D. B. Plasmonic-metal nanostructures for efficient conversion of solar to chemical energy. *Nat. Mater.* **2011**, *10*, 911–921.

[59] Li, J.; Ye, Y. H.; Ye, L. Q.; Su, F. Y.; Ma, Z. Y.; Huang, J. D.; Xie, H. Q.; Doronkin, D. E.; Zimina, A.; Grunwaldt, J. D. et al. Sunlight induced photo-thermal synergistic catalytic CO_2 conversion via localized surface plasmon resonance of MoO_{3-x}. *J. Mater. Chem. A* **2019**, *7*, 2821–2830.

[60] Guo, L.; Sun, Q.; Marcus, K.; Hao, Y.; Deng, J.; Bi, K.; Yang, Y. Photocatalytic glycerol oxidation on Au_xCu-CuS@TiO_2 plasmonic heterostructures. *J. Mater. Chem. A* **2018**, *6*, 22005–22012.

[61] Gan, Z. X.; Wu, X. L.; Meng, M.; Zhu, X. B.; Yang, L.; Chu, P. K. Photothermal contribution to enhanced photocatalytic performance of graphene-based nanocomposites. *ACS Nano* **2014**, *8*, 9304–9310.

[62] Ng, S. W. L.; Gao, M. M.; Lu, W. H.; Hong, M. H.; Ho, G. W. Selective wavelength enhanced photochemical and photothermal H_2 generation of classical oxide supported metal catalyst. *Adv. Funct. Mater.* **2021**, *31*, 2104750.

[63] Wang, L.; Dong, Y. C.; Yan, T. J.; Hu, Z. X.; Jelle, A. A.; Meira, D. M.; Duchesne, P. N.; Loh, J. Y. Y.; Qiu, C. Y.; Storey, E. E. et al. Black indium oxide a photothermal CO_2 hydrogenation catalyst. *Nat. Commun.* **2020**, *11*, 2432.

[64] Yang, M. Q.; Shen, L.; Lu, Y. Y.; Chee, S. W.; Lu, X.; Chi, X.; Chen, Z. H.; Xu, Q. H.; Mirsaidov, U.; Ho, G. W. Disorder engineering in monolayer nanosheets enabling photothermic catalysis for full solar spectrum (250–2500 nm) harvesting. *Angew. Chem., Int. Ed.* **2019**, *58*, 3077–3081.

[65] Jia, J.; Wang, H.; Lu, Z. L.; O'Brien, P. G.; Ghoussoub, M.; Duchesne, P.; Zheng, Z. Q.; Li, P. C.; Qiao, Q.; Wang, L. et al. Photothermal catalyst engineering: Hydrogenation of gaseous CO_2 with high activity and tailored selectivity. *Adv. Sci.* **2017**, *4*, 1700252.

[66] Sun, M. Y.; Zhao, B. H.; Chen, F. P.; Liu, C. B.; Lu, S. Y.; Yu, Y. F.; Zhang, B. Thermally-assisted photocatalytic CO_2 reduction to fuels. *Chem. Eng. J.* **2021**, *408*, 127280.

[67] Song, H.; Luo, S. Q.; Huang, H. M.; Deng, B. W.; Ye, J. H. Solar-driven hydrogen production: Recent advances, challenges, and future perspectives. *ACS Energy Lett.* **2022**, *7*, 1043–1065.

[68] Li, P. Y.; Liu, L.; An, W. J.; Wang, H.; Guo, H. X.; Liang, Y. H.; Cui, W. Q. Ultrathin porous g-C_3N_4 nanosheets modified with AuCu alloy nanoparticles and C–C coupling photothermal catalytic reduction of CO_2 to ethanol. *Appl. Catal. B:Environ.* **2020**, *266*, 118618.

[69] Liu, D. L.; Xu, Y.; Sun, M. Y.; Huang, Y.; Yu, Y. F.; Zhang, B. Photothermally assisted photocatalytic conversion of CO_2-H_2O into fuels over a WN-WO_3 Z-scheme heterostructure. *J. Mater. Chem. A* **2020**, *8*, 1077–1083.

[70] Ghuman, K. K.; Wood, T. E.; Hoch, L. B.; Mims, C. A.; Ozin, G. A.; Singh, C. V. Illuminating CO_2 reduction on frustrated Lewis pair surfaces: Investigating the role of surface hydroxides and oxygen vacancies on nanocrystalline $In_2O_{(3-x)}(OH)_y$. *Phys. Chem. Chem. Phys.* **2015**, *17*, 14623–14635.

[71] Ghuman, K. K.; Hoch, L. B.; Szymanski, P.; Loh, J. Y. Y.; Kherani, N. P.; El-Sayed, M. A.; Ozin, G. A.; Singh, C. V. Photoexcited surface frustrated Lewis pairs for heterogeneous photocatalytic CO_2 reduction. *J. Am. Chem. Soc.* **2016**, *138*, 1206–1214.

[72] Yu, F.; Wang, C. H.; Li, Y. Y.; Ma, H.; Wang, R.; Liu, Y. C.; Suzuki, N.; Terashima, C.; Ohtani, B.; Ochiai, T. et al. Enhanced solar photothermal catalysis over solution plasma activated TiO_2. *Adv. Sci.* **2020**, *7*, 2000204.

[73] Ling, L. L.; Yang, W. J.; Yan, P.; Wang, M.; Jiang, H. L. Light-assisted CO_2 hydrogenation over Pd_3Cu@UiO-66 promoted by active sites in close proximity. *Angew. Chem., Int. Ed.* **2022**, *61*, e202116396.

[74] Liu, H. M.; Meng, X. G.; Dao, T. D.; Zhang, H. B.; Li, P.; Chang, K.; Wang, T.; Li, M.; Nagao, T.; Ye, J. H. Conversion of carbon dioxide by methane reforming under visible-light irradiation: Surface-plasmon-mediated nonpolar molecule activation. *Angew. Chem., Int. Ed.* **2015**, *54*, 11545–11549.

[75] Lu, B. W.; Quan, F. J.; Sun, Z.; Jia, F. L.; Zhang, L. Z. Photothermal reverse-water-gas-shift over Au/CeO_2 with high yield and selectivity in CO_2 conversion. *Catal. Commun.* **2019**, *129*, 105724.

[76] Liu, H. M.; Li, M.; Dao, T. D.; Liu, Y. Y.; Zhou, W.; Liu, L. Q.; Meng, X. G.; Nagao, T.; Ye, J. H. Design of PdAu alloy plasmonic nanoparticles for improved catalytic performance in CO_2 reduction with visible light irradiation. *Nano Energy* **2016**, *26*, 398–404.

[77] Song, H.; Meng, X. G.; Dao, T. D.; Zhou, W.; Liu, H. M.; Shi, L.; Zhang, H. B.; Nagao, T.; Kako, T.; Ye, J. H. Light-enhanced carbon dioxide activation and conversion by effective plasmonic coupling effect of Pt and Au nanoparticles. *ACS Appl. Mater. Interfaces* **2018**, *10*, 408–416.

[78] Xu, C. Y.; Huang, W. H.; Li, Z.; Deng, B. W.; Zhang, Y. W.; Ni, M. J.; Cen, K. F. Photothermal coupling factor achieving CO_2 reduction based on palladium-nanoparticle-loaded TiO_2. *ACS Catal.* **2018**, *8*, 6582–6593.

[79] Docao, S.; Koirala, A. R.; Kim, M. G.; Hwang, I. C.; Song, M. K.; Yoon, K. B. Solar photochemical-thermal water splitting at 140 °C with Cu-loaded TiO_2. *Energy Environ. Sci.* **2017**, *10*, 628–640.

[80] Zhou, L. N.; Martirez, J. M. P.; Finzel, J.; Zhang, C.; Swearer, D. F.; Tian, S.; Robatjazi, H.; Lou, M. H.; Dong, L. L.; Henderson, L.

et al. Light-driven methane dry reforming with single atomic site antenna-reactor plasmonic photocatalysts. *Nat. Energy* **2020**, *5*, 61–70.

[81] Jia, J.; O'Brien, P. G.; He, L.; Qiao, Q.; Fei, T.; Reyes, L. M.; Burrow, T. E.; Dong, Y. C.; Liao, K.; Varela, M. et al. Visible and near-infrared photothermal catalyzed hydrogenation of gaseous CO_2 over nanostructured Pd@Nb_2O_5. *Adv. Sci.* **2016**, *3*, 1600189.

[82] Mateo, D.; Albero, J.; García, H. Graphene supported NiO/Ni nanoparticles as efficient photocatalyst for gas phase CO_2 reduction with hydrogen. *Appl. Catal. B:Environ.* **2018**, *224*, 563–571.

[83] Pan, F. P.; Xiang, X. M.; Du, Z. C.; Sarnello, E.; Li, T.; Li, Y. Integrating photocatalysis and thermocatalysis to enable efficient CO_2 reforming of methane on Pt supported CeO_2 with Zn doping and atomic layer deposited MgO overcoating. *Appl. Catal. B:Environ.* **2020**, *260*, 118189.

[84] Zhang, G. Q.; Wu, S. W.; Li, Y. Z.; Zhang, Q. Significant improvement in activity, durability, and light-to-fuel efficiency of Ni nanoparticles by La_2O_3 cluster modification for photothermocatalytic CO_2 reduction. *Appl. Catal. B:Environ.* **2020**, *264*, 118544.

[85] Yang, H.; He, L. Q.; Hu, Y. W.; Lu, X. H.; Li, G. R.; Liu, B. J.; Ren, B.; Tong, Y. X.; Fang, P. P. Quantitative detection of photothermal and photoelectrocatalytic effects induced by SPR from Au@Pt nanoparticles. *Angew. Chem., Int. Ed.* **2015**, *54*, 11462–11466.

[86] Zhang, X.; Li, X. Q.; Reish, M. E.; Zhang, D.; Su, N. Q.; Gutiérrez, Y.; Moreno, F.; Yang, W. T.; Everitt, H. O.; Liu, J. Plasmon-enhanced catalysis: Distinguishing thermal and nonthermal effects. *Nano Lett.* **2018**, *18*, 1714–1723.

[87] Gao, M. M.; Peh, C. K.; Zhu, L. L.; Yilmaz, G.; Ho, G. W. Photothermal catalytic gel featuring spectral and thermal management for parallel freshwater and hydrogen production. *Adv. Energy Mater.* **2020**, *10*, 2000925.

[88] Huang, H.; Mao, M. Y.; Zhang, Q.; Li, Y. Z.; Bai, J. L.; Yang, Y.; Zeng, M.; Zhao, X. J. Solar-light-driven CO_2 reduction by CH_4 on silica-cluster-modified Ni nanocrystals with a high solar-to-fuel efficiency and excellent durability. *Adv. Energy Mater.* **2018**, *8*, 1702472.

[89] Li, X. Q.; Everitt, H. O.; Liu, J. Confirming nonthermal plasmonic effects enhance CO_2 methanation on Rh/TiO_2 catalysts. *Nano Res.* **2019**, *12*, 1906–1911.

[90] Robatjazi, H.; Zhao, H. Q.; Swearer, D. F.; Hogan, N. J.; Zhou, L. N.; Alabastri, A.; McClain, M. J.; Nordlander, P.; Halas, N. J. Plasmon-induced selective carbon dioxide conversion on earth-abundant aluminum-cuprous oxide antenna-reactor nanoparticles. *Nat. Commun.* **2017**, *8*, 27.

[91] Cai, M. J.; Wu, Z. Y.; Li, Z.; Wang, L.; Sun, W.; Tountas, A. A.; Li, C. R.; Wang, S. H.; Feng, K.; Xu, A. B. et al. Greenhouse-inspired supra-photothermal CO_2 catalysis. *Nat. Energy* **2021**, *6*, 807–814.

[92] Li, Y. G.; Hao, J. C.; Song, H.; Zhang, F. Y.; Bai, X. H.; Meng, X. G.; Zhang, H. Y.; Wang, S. F.; Hu, Y.; Ye, J. H. Selective light absorber-assisted single nickel atom catalysts for ambient sunlight-driven CO_2 methanation. *Nat. Commun.* **2019**, *10*, 2359.

[93] Wang, Q.; Pornrungroj, C.; Linley, S.; Reisner, E. Strategies to improve light utilization in solar fuel synthesis. *Nat. Energy* **2022**, *7*, 13–24.

[94] Menges, F.; Mensch, P.; Schmid, H.; Riel, H.; Stemmer, A.; Gotsmann, B. Temperature mapping of operating nanoscale devices by scanning probe thermometry. *Nat. Commun.* **2016**, *7*, 10874.

[95] Mecklenburg, M.; Hubbard, W. A.; White, E. R.; Dhall, R.; Ronin, S. B.; Aloni, S.; Regan, B. C. Nanoscale temperature mapping in operating microelectronic devices. *Science,* **2015**, *347*, 629–632.

[96] Barella, M.; Violi, I. L.; Gargiulo, J.; Martinez, L. P.; Goschin, F.; Guglielmotti, V.; Pallarola, D.; Schlücker, S.; Pilo-Pais, M.; Acuna, G. P. et al. *In situ* photothermal response of single gold nanoparticles through hyperspectral imaging anti-Stokes thermometry. *ACS Nano* **2021**, *15*, 2458–2467.

[97] Feng, K.; Wang, S. H.; Zhang, D. K.; Wang, L.; Yu, Y. Y.; Feng, K.; Li, Z.; Zhu, Z. J.; Li, C. R.; Cai, M. J. et al. Cobalt plasmonic superstructures enable almost 100% broadband photon efficient CO_2 photocatalysis. *Adv. Mater.* **2020**, *32*, 2000014.

[98] Mao, C. L.; Li, H.; Gu, H. G.; Wang, J. X.; Zou, Y. J.; Qi, G. D.; Xu, J.; Deng, F.; Shen, W. J.; Li, J. et al. Beyond the thermal equilibrium limit of ammonia synthesis with dual temperature zone catalyst powered by solar light. *Chem* **2019**, *5*, 2702–2717.

[99] Xie, S. B.; Iglesia, E.; Bell, A. T. Effects of temperature on the Raman spectra and dispersed oxides. *J. Phys. Chem. B* **2001**, *105*, 5144–5152.

[100] Song, C. Q.; Liu, X.; Xu, M.; Masi, D.; Wang, Y. G.; Deng, Y. C.; Zhang, M. T.; Qin, X. T.; Feng, K.; Yan, J. et al. Photothermal conversion of CO_2 with tunable selectivity using Fe-based catalysts: From oxide to carbide. *ACS Catal.* **2020**, *10*, 10364–10374.

[101] Westrich, T. A.; Dahlberg, K. A.; Kaviany, M.; Schwank, J. W. High-temperature photocatalytic ethylene oxidation over TiO_2. *J. Phys. Chem. C* **2011**, *115*, 16537–16543.

[102] Mahmoud, M. A. Reducing the photocatalysis induced by hot electrons of plasmonic nanoparticles due to tradeoff of photothermal heating. *Phys. Chem. Chem. Phys.* **2017**, *19*, 32016–32023.

[103] Li, Y.; Li, R. Z.; Li, Z. H.; Wei, W. Q.; Ouyang, S. X.; Yuan, H.; Zhang, T. R. Effect of support on catalytic performance of photothermal Fischer–Tropsch synthesis to produce lower olefins over Fe_5C_2-based catalysts. *Chem. Res. Chin. Univ.* **2020**, *36*, 1006–1012.

[104] Zhang, D. K.; Lv, K. X.; Li, C. R.; Fang, Y. S.; Wang, S. H.; Chen, Z. J.; Wu, Z. Y.; Guan, W. H.; Lou, D. Y.; Sun, W. et al. All-earth-abundant photothermal silicon platform for CO_2 catalysis with nearly 100% sunlight harvesting ability. *Sol. RRL* **2021**, *5*, 2000387.

[105] Zhang, Z. S.; Mao, C. L.; Meira, D. M.; Duchesne, P. N.; Tountas, A. A.; Li, Z.; Qiu, C. Y.; Tang, S. L.; Song, R.; Ding, X. et al. New black indium oxide-tandem photothermal CO_2-H_2 methanol selective catalyst. *Nat. Commun.* **2022**, *13*, 1512.

[106] Ulmer, U.; Dingle, T.; Duchesne, P. N.; Morris, R. H.; Tavasoli, A.; Wood, T.; Ozin, G. A. Fundamentals and applications of photocatalytic CO_2 methanation. *Nat. Commun.* **2019**, *10*, 3169.

[107] Cai, M. J.; Li, C. R.; He, L. Enhancing photothermal CO_2 catalysis by thermal insulating substrates. *Rare Met.* **2020**, *39*, 881–886.

[108] Kong, N.; Han, B.; Li, Z.; Fang, Y. S.; Feng, K.; Wu, Z. Y.; Wang, S. H.; Xu, A. B.; Yu, Y. Y.; Li, C. R. et al. Ruthenium nanoparticles supported on $Mg(OH)_2$ microflowers as catalysts for photothermal carbon dioxide hydrogenation. *ACS Appl. Nano Mater.* **2020**, *3*, 3028–3033.

[109] Liu, G. G.; Meng, X. G.; Zhang, H. B.; Zhao, G. X.; Pang, H.; Wang, T.; Li, P.; Kako, T.; Ye, J. H. Elemental boron for efficient carbon dioxide reduction under light irradiation. *Angew. Chem., Int. Ed.* **2017**, *56*, 5570–5574.

[110] Ren, J.; Ouyang, S. X.; Xu, H.; Meng, X. G.; Wang, T.; Wang, D. F.; Ye, J. H. Targeting activation of CO_2 and H_2 over Ru-loaded ultrathin layered double hydroxides to achieve efficient photothermal CO_2 methanation in flow-type system. *Adv. Energy Mater.* **2017**, *7*, 1601657.

[111] Wu, Z. Y.; Li, C. R.; Li, Z.; Feng, K.; Cai, M. J.; Zhang, D. K.; Wang, S. H.; Chu, M. Y.; Zhang, C. C.; Shen, J. H. et al. Niobium and titanium carbides (MXenes) as superior photothermal supports for CO_2 photocatalysis. *ACS Nano* **2021**, *15*, 5696–5705.

[112] Mateo, D.; Albero, J.; García, H. Titanium-perovskite-supported RuO_2 nanoparticles for photocatalytic CO_2 methanation. *Joule* **2019**, *3*, 1949–1962.

[113] Cho, Y.; Shoji, S.; Yamaguchi, A.; Hoshina, T.; Fujita, T.; Abe, H.; Miyauchi, M. Visible-light-driven dry reforming of methane using a semiconductor-supported catalyst. *Chem. Commun.* **2020**, *56*, 4611–4614.

[114] Li, Y.; Xue, J. B.; Shen, Q. Q.; Jia, S. F.; Li, Q.; Li, Y. X.; Liu, X. G.; Jia, H. S. Construction of a ternary spatial junction in yolk–shell nanoreactor for efficient photo-thermal catalytic hydrogen generation. *Chem. Eng. J.* **2021**, *423*, 130188.

[115] Zhang, H. W.; Itoi, T.; Konishi, T.; Izumi, Y. Dual photocatalytic

roles of light: Charge separation at the band gap and heat via localized surface plasmon resonance to convert CO_2 into CO over silver-zirconium oxide. *J. Am. Chem. Soc.* **2019**, *141*, 6292–6301.

[116] Song, R.; Luo, B.; Geng, J. F.; Song, D. X.; Jing, D. W. Photothermocatalytic hydrogen evolution over Ni_2P/TiO_2 for full-spectrum solar energy conversion. *Ind. Eng. Chem. Res.* **2018**, *57*, 7846–7854.

[117] Caudillo-Flores, U.; Agostini, G.; Marini, C.; Kubacka, A.; Fernández-García, M. Hydrogen thermo-photo production using Ru/TiO_2: Heat and light synergistic effects. *Appl. Catal. B:Environ.* **2019**, *256*, 117790.

[118] Fang, S. Y.; Sun, Z. X.; Hu, Y. H. Insights into the thermo-photo catalytic production of hydrogen from water on a low-cost NiO_x-loaded TiO_2 catalyst. *ACS Catal.* **2019**, *9*, 5047–5056.

[119] Ha, M. N.; Lu, G. Z.; Liu, Z. F.; Wang, L. C.; Zhao, Z. 3DOM-$LaSrCoFeO_{6-\delta}$ as a highly active catalyst for the thermal and photothermal reduction of CO_2 with H_2O to CH_4. *J. Mater. Chem. A* **2016**, *4*, 13155–13165.

[120] Wang, L. C.; Wang, Y.; Cheng, Y.; Liu, Z. F.; Guo, Q. S.; Ha, M. N.; Zhao, Z. Hydrogen-treated mesoporous WO_3 as a reducing agent of CO_2 to fuels (CH_4 and CH_3OH) with enhanced photothermal catalytic performance. *J. Mater. Chem. A* **2016**, *4*, 5314–5322.

[121] Lin, L. L.; Wang, K.; Yang, K.; Chen, X.; Fu, X. Z.; Dai, W. X. The visible-light-assisted thermocatalytic methanation of CO_2 over $Ru/TiO_{(2-x)}N_x$. *Appl. Catal. B:Environ.* **2017**, *204*, 440–455.

[122] Zhang, H. B.; Wang, T.; Wang, J. J.; Liu, H. M.; Dao, T. D.; Li, M.; Liu, G. G.; Meng, X. G.; Chang, K.; Shi, L. et al. Surface-plasmon-enhanced photodriven CO_2 reduction catalyzed by metal-organic-framework-derived iron nanoparticles encapsulated by ultrathin carbon layers. *Adv. Mater.* **2016**, *28*, 3703–3710.

[123] Wang, Z. J.; Song, H.; Pang, H.; Ning, Y. X.; Dao, T. D.; Wang, Z.; Chen, H. L.; Weng, Y. X.; Fu, Q.; Nagao, T. et al. Photo-assisted methanol synthesis via CO_2 reduction under ambient pressure over plasmonic Cu/ZnO catalysts. *Appl. Catal. B: Environ.* **2019**, *250*, 10–16.

[124] Wang, L.; Ghoussoub, M.; Wang, H.; Shao, Y.; Sun, W.; Tountas, A. A.; Wood, T. E.; Li, H.; Loh, J. Y. Y.; Dong, Y. C. et al. Photocatalytic hydrogenation of carbon dioxide with high selectivity to methanol at atmospheric pressure. *Joule* **2018**, *2*, 1369–1381.

[125] Han, K. H.; Wang, Y.; Wang, S.; Liu, Q. Y.; Deng, Z. Y.; Wang, F. G. Narrowing band gap energy of CeO_2 in $(Ni/CeO_2)@SiO_2$ catalyst for photothermal methane dry reforming. *Chem. Eng. J.* **2021**, *421*, 129989.

[126] Wang, C.; Su, Y.; Tavasoli, A.; Sun, W.; Wang, L.; Ozin, G. A.; Yang, D. Recent advances in nanostructured catalysts for photo-assisted dry reforming of methane. *Mater. Today Nano* **2021**, *14*, 100113.

[127] Liu, H. M.; Song, H.; Zhou, W.; Meng, X. G.; Ye, J. H. A promising application of optical hexagonal TaN in photocatalytic reactions. *Angew. Chem., Int. Ed.* **2018**, *57*, 16781–16784.

[128] Li, Z. H.; Shi, R.; Zhao, J. Q.; Zhang, T. R. Ni-based catalysts derived from layered-double-hydroxide nanosheets for efficient photothermal CO_2 reduction under flow-type system. *Nano Res.* **2021**, *14*, 4828–4832.

[129] Liu, H. M.; Meng, X. G.; Dao, T. D.; Liu, L. Q.; Li, P.; Zhao, G. X.; Nagao, T.; Yang, L. Q.; Ye, J. H. Light assisted CO_2 reduction with methane over SiO_2 encapsulated Ni nanocatalysts for boosted activity and stability. *J. Mater. Chem. A* **2017**, *5*, 10567–10573.

[130] Sun, W.; Cao, X. E. Photothermal CO_2 catalysis: From catalyst discovery to reactor design. *Chem Catal.* **2022**, *2*, 215–217.

[131] Cao, X. E.; Kaminer, Y.; Hong, T.; Schein, P.; Liu, T. W.; Hanrath, T.; Erickson, D. HI-Light: A glass-waveguide-based "shell-and-tube" photothermal reactor platform for converting CO_2 to fuels. *iScience* **2020**, *23*, 101856.